Tracing marine cryptotephras in the North Atlantic during the Last Glacial Period: Improving the North Atlantic marine tephra framework

Peter M. Abbott[1,2,3,*], Adam J. Griggs[1], Anna J. Bourne[1,4], Mark R. Chapman[5], Siwan M. Davies[1]

[1]Department of Geography, College of Science, Swansea University, Singleton Park, Swansea, SA2 8PP, UK

[2]School of Earth and Ocean Sciences, Cardiff University, Park Place, CF10 3AT, Cardiff, UK

[3]Institute of Geological Sciences and Oeschger Center for Climate Change Research, University of Bern, Baltzerstrasse 1+3, Bern 3012, Switzerland

[4]Geography and Environment, University of Southampton, University Road, Southampton, SO17 1BJ, UK

[5]School of Environmental Sciences, University of East Anglia, Norwich Research Park, NR4 7TJ, UK

*Corresponding author (abbottp@cardiff.ac.uk)

1   **Tracing marine cryptotephras in the North Atlantic during the Last Glacial Period:**

2   **Improving the North Atlantic marine tephra framework**

3

4   Peter M. Abbott[1,2,3,*], Adam J. Griggs[1], Anna J. Bourne[1,4], Mark R. Chapman[5], Siwan M.

5   Davies[1]

6

7   [1]Department of Geography, College of Science, Swansea University, Singleton Park,

8   Swansea, SA2 8PP, UK

9   [2]School of Earth and Ocean Sciences, Cardiff University, Park Place, CF10 3AT, Cardiff, UK

10   [3]Institute of Geological Sciences and Oeschger Center for Climate Change Research,

11   University of Bern, Baltzerstrasse 1+3, Bern 3012, Switzerland

12   [4]Geography and Environment, University of Southampton, University Road, Southampton,

13   SO17 1BJ, UK

14   [5]School of Environmental Sciences, University of East Anglia, Norwich Research Park, NR4

15   7TJ, UK

16

17   *Corresponding author (abbottp@cardiff.ac.uk)

18

19   ***Abstract***

20

21   Tephrochronology is increasingly being recognised as a key tool for the correlation of

22   disparate palaeoclimatic archives, underpinning chronological models and facilitating

23   climatically independent comparisons of climate proxies. Tephra frameworks integrating both

24   distal and proximal tephra occurrences are essential to these investigations providing key

25   information on their spatial distributions, geochemical signatures, eruptive sources as well as

26   any available chronological and/or stratigraphic information. Frameworks also help to avoid

27   mis-correlation of horizons and provide important information on volcanic history. Here we

28   present a comprehensive framework of 14 tephra horizons from North Atlantic marine

29   sequences spanning 25-60 ka BP. Horizons previously discovered as visible or coarse-grained

30   deposits have been combined with 11 newly recognised volcanic events, identified through

31   the application of cryptotephra identification and characterisation methods to a wide network

32   of marine sequences. Their isochronous integrity has been assessed using their physical

33   characteristics. All horizons originated from Iceland with the vast majority having a basaltic

34   composition sourced from the Grímsvötn, Kverkfjöll, Hekla/Vatnafjöll and Katla volcanic

35 systems. New occurrences, improved stratigraphic placements and a refinement of the

36 geochemical signature of the NAAZ II are reported and the range of the FMAZ IV has been

37 extended. In addition, several significant geochemical populations that further investigations

38 could show to be isochronous are reported. This tephra framework provides the foundation

39 for the correlation and synchronisation of these marine records to the Greenland ice-cores and

40 European terrestrial records to investigate the phasing, rate, timing and mechanisms

41 controlling the rapid climate changes that characterised the last glacial period.

42

43 **Keywords:** Quaternary; palaeoceanography; tephrochronology; North Atlantic; tephra

44 framework; marine cores

45

46 *1. Introduction*

47

48 Tephrochronology, the use of volcanic ash deposits as tie-lines between disparate

49 palaeoclimatic records, is increasingly being utilised as a key geochronological tool for

50 reconstructing the timing and phasing of past climatic events (e.g. Lowe, 2011; Lowe et al.,

51 2012; Lane et al., 2013; Davies, 2015). This upsurge is directly linked to advances in

52 cryptotephra analysis, which has dramatically increased the number of potential tie-lines and

53 led to the compilation of regional tephra frameworks that underpin correlations and are key

54 datasets for future tephrochronological studies (e.g. Lowe et al., 2008; Tyron et al., 2009;

55 Zanchetta et al., 2011; Davies et al., 2012; Abbott and Davies, 2012; Lowe et al., 2015).

56 Tephrostratigraphical frameworks typically include a compilation of key information relating

57 to the tephra horizons within them, including their spatial extent, based on preservation

58 within proxy records, tephra shard concentrations, glass shard composition and eruptive

59 source alongside chronological and stratigraphic information (e.g. Davies et al., 2014; Bourne

60 et al., 2015; Matthews et al., 2015). The most comprehensive frameworks include both distal

61 and proximal tephra findings, visible and cryptotephra tephra occurrences and combine newly

62 discovered data with previously published deposits. Integrating all this information can

63 provide valuable frameworks for the volcanic history of a region and provide key reference

64 tools for future studies. Distal archives are often more complete than proximal records, that

65 are prone to removal or burial of deposits, while proximal archives can often record more

66 information regarding eruptions, such as their full geochemical evolution. In addition,

67 developing the most comprehensive tephra frameworks will help to reduce instances of mis-

2

68   correlation which can occur if volcanic regions produce multiple, closely-timed eruptions

69   with similar geochemical compositions (e.g. Bourne et al., 2013).

70

71   For the North Atlantic region a number of detailed frameworks spanning a range of time-

72   intervals are currently available. For example, Gudmundsdottir et al. (2016) provides a

73   proximal framework of Icelandic eruptions during the Holocene, Blockley et al. (2014)

74   summarises the European tephra stratigraphy over the last glacial cycle and Davies et al.

75   (2014) provides an integrated framework of MIS 5 tephras in Greenland ice-cores and North

76   Atlantic marine records. The tephra framework for the Greenland ice-cores has significantly

77   expanded in recent years (e.g. Mortensen et al., 2005; Abbott and Davies, 2012; Davies et al.,

78   2014), in particular over the MIS 2-3 period (Bourne et al., 2015), highlighting the value of

79   exploring these distal archives. In comparison, however, a limited number of tephra horizons

80   have been identified in North Atlantic marine records spanning MIS 2-3 (see Haflidason et

81   al., 2000; Wastegård et al., 2006; Section 2). This is despite considerable advances in distal

82   tephrochronology and the high potential for a tephra framework from these sequences to be

83   used to establish correlations to the Greenland ice-cores and European terrestrial records.

84   Such correlations could help answer key questions regarding the relative timing of

85   atmospheric and oceanic changes associated with the rapid climatic events, that punctuated

86   the region during the last glacial period (e.g. NGRIP Members, 2004; Bond et al., 1993;

87   Martrat et al., 2007; Hall et al., 2011; Zumaque et al., 2012; Henry et al., 2016).

88

89   Here we present a tephra framework for North Atlantic marine records spanning MIS 2-3,

90   which is underpinned by our investigations of an extensive core network (Figure 1) using

91   recently developed cryptotephra identification methods (Abbott et al., submitted). Prior

92   studies are also reviewed (Section 2) and previously identified isochronous horizons are

93   integrated with our new cryptotephra discoveries. This represents the most concerted attempt

94   to improve the tephra framework for the North Atlantic and overall a framework of 14 marine

95   tephra horizons between 25-60 ka BP has been defined (Figure 2). This framework

96   significantly enhances the potential to establish further correlations within the North Atlantic

97   Ocean as well as to ice-core and terrestrial records.

98

99   ***2. Prior North Atlantic Tephra Investigations between 25-60 ka BP***

100

101　It was highlighted earlier that tephra frameworks should integrate all isochronous tephra

102　deposits from a region and, as such, the framework presented in this work integrates our new

103　discoveries alongside previously published data from multiple cores sites from the North

104　Atlantic (green sites on Figure 1). Within these prior tephrochronological studies of the MIS

105　2-3 period several isochronous tephra horizons have been identified, i.e. North Atlantic Ash

106　Zone II (NAAZ II), Faroe Marine Ash Zone (FMAZ) II and FMAZ IV. Reviewing the

107　literature does, however, highlight some of the challenges associated with determining the

108　isochronous nature of deposits and the limitations of earlier studies that only focused on the

109　coarse fraction (>150 μm) of the sediments. These were the major factors driving the

110　development of a procedure for isolating fine-grained cryptotephras (down to 25 μm

111　diameter) and interpreting transportation and depositional processes (e.g. Abbott et al., 2011,

112　submitted; Davies et al., 2014; Griggs et al., 2014). The latter is essential for determining the

113　isochronous nature of fine-grained, cryptotephra deposits for which macro-sedimentary

114　evidence cannot be utilised to determine the relative influence of primary and secondary

115　processes. These methods were utilised by Abbott et al. (2016) to identify three previously

116　undocumented MIS 2-3 volcanic events within a core retrieved from the Goban Spur (see

117　Section 4 for details) and are more widely applied in this study.

118

119　The first MIS 3 tephra deposit to be recognised in the North Atlantic was NAAZ II, first

120　identified by Bramlette and Bradley (1941) and later described by Ruddiman and Glover

121　(1972). This is a complex ash zone composed of the products of several Icelandic eruptions

122　(see Section 4.1.1) with rhyolitic material from one eruption (II-RHY-1) the most

123　widespread, being traced into multiple marine cores and the Greenland ice-cores (e.g.

124　Kvamme et al., 1989; Lacasse et al., 1996; Haflidason et al., 2000; Austin et al., 2004;

125　Grönvold et al., 1995; Zielinski et al., 1997; Svensson et al., 2008). This widespread nature

126　gives rise to a key tie-line between North Atlantic marine records and the Greenland ice-cores

127　within the North Atlantic tephra framework (Austin and Abbott, 2010).

128

129　The FMAZs are a series of ash zones identified in cores around the Faroe Islands region, and

130　three, II, III and IV, were deposited during MIS 2-3. Two of these, FMAZ II and IV, have

131　isochronous characteristics and are integrated within the framework (Figures 1 and 2;

132　Rasmussen et al., 2003; Wastegård et al., 2006; Wastegård and Rasmussen, 2014; Griggs et

133　al., 2014). FMAZ II was described by Wastegård et al. (2006) as a visible horizon and was

134　suggested to be a widespread primary airfall deposit. The FMAZ II was subsequently traced

135   into the NGRIP ice-core by Davies et al. (2008) (NGRIP 1848 m; 26,740 ± 390 yr b2k),

136   providing a clear demonstration of the high potential for ice-marine correlations between the

137   Greenland ice-cores and North Atlantic marine sequences during the 25-60 ka BP period.

138   FMAZ IV was first described by Wastegård and Rasmussen (2014) as a layer up to 20 cm

139   thick deposited shortly after warming related to Dansgaard-Oeschger (DO) event 12. Due to

140   its homogenous composition and micro-sedimentary features (Griggs et al., 2014, 2015) it

141   has been interpreted as a primary airfall deposit.

142

143   FMAZ III, identified as a thick relatively scattered zone of tephra in the Faroes cores, was

144   also thought to have a correlative in the NGRIP core (NGRIP 2066.95 m; 38,122 ± 723 yr

145   b2k; Davies et al., 2010). However, Bourne et al. (2013) subsequently identified a series of

146   closely-spaced tephra horizons in the NGRIP and NEEM ice-cores around NGRIP 2066.95

147   m, many with geochemical compositions that fall within the wide geochemical envelope of

148   FMAZ III. This highlighted the complexity of the period and demonstrated that the suggested

149   correlation was inappropriate and did not represent an ice-marine tie-line (Bourne et al.,

150   2013). Bourne et al. (2013) and Griggs et al. (2014) both suggested that FMAZ III formed

151   through the amalgamation of tephra due to several closely spaced volcanic events and low

152   sedimentation rates at the core sites and as such is not incorporated in the marine tephra

153   framework.

154

155   Early studies of North Atlantic tephra mainly focused on investigating visible tephra horizons

156   or tephra shards present within the coarse fraction of the sediment (i.e. >150 μm diameter).

157   This may have created a bias towards the identification of horizons from large scale eruptions

158   and/or horizons not deposited via primary airfall (Brendryen et al., 2010; Abbott et al., 2011).

159   The study of Lackschewitz and Wallrabe-Adams (1997) highlights the limitation of this

160   approach. Several ash zones above NAAZ II were identified within and correlated between a

161   series of cores from the Reykjanes Ridge, however, most of these deposits have

162   heterogeneous geochemical compositions and in general coincide with distinct peaks in ice-

163   rafted debris (IRD). Based on these factors Lackschewitz and Wallrabe-Adams (1997)

164   concluded that this material was transported to the sites via iceberg rafting. This process

165   could have significantly delayed the deposition of these deposits and, as such, they do not

166   represent isochronous marker horizons and are not incorporated in the marine tephra

167   framework. The only deposit with isochronous characteristics was the VZ 1x peak, a discrete

168   high concentration peak within VZ 1 in the SO82-5 core, with a homogenous composition

169 and no coeval IRD peak. This horizon was subsequently correlated to FMAZ II by Wastegård

170 et al. (2006) (Figure 2).

171

172 Voelker and Haflidason (2015) utilised the coarse sediment fraction to define a high-

173 resolution tephrochronology for the last 86 ka from the southern Greenland Sea PS2644 core.

174 This sequence was interpreted as containing a record of 68 volcanic events between ~25-60

175 ka BP based on the geochemical analysis of glass shards from 28 depths in the core. The

176 volcanic events, however, are sometimes defined based on a limited number of geochemical

177 analyses with multiple geochemical populations/events often identified at the same depth.

178 According to protocols for assessing deposits this could be indicative of deposition via

179 iceberg rafting and/or secondary depositional processes (Abbott et al., submitted), however,

180 while these processes were acknowledged a distinction between tephra deposited via primary

181 or secondary process is often not made. This may have led to the overreporting of the number

182 of isochronous deposits present and, as such, these volcanic events are not incorporated into

183 the North Atlantic tephra framework presented here. However, it is important to note these

184 findings as a reappraisal of these deposits together with IRD evidence may well reveal the

185 presence of dominant populations and valuable isochrons in the future.

186

187 *3. Methodology*

188

189 *3.1 Detecting, characterising and correlating cryptotephra deposits*

190

191 A widespread network of North Atlantic cores was investigated (Figure 1) and we applied the

192 consistent methodological approach for cryptotephra identification outlined in Abbott et al.

193 (submitted). Following preliminary low-resolution analysis high-resolution glass shard

194 concentration profiles were gained from the core deposits. The major element composition of

195 peaks in glass shard concentrations were characterised using electron-probe micro-analysis

196 (EPMA) with at least 20-40 individual shards from each deposit analysed (see Abbott et al.,

197 submitted for full description). For all analysis and data comparison the major element data

198 were normalised to an anhydrous basis, i.e. 100 % total oxides, however, the raw

199 geochemical data are provided in the Supplementary Data alongside secondary standard

200 analyses (Table S12). Potential sources for geochemical populations and tephra horizons

201 were explored through graphical comparison of the composition of individual shards with

202 glass and whole rock analyses from proximal Holocene Icelandic deposits from the three

6

203 different rock suites and specific volcanic systems. We acknowledge that some centres may

204 have geochemically evolved or not been productive during the last glacial period, therefore,

205 the potential sources proposed here could be revised.

206

207 Potential cross-correlations between all the isochronous horizons and significant geochemical

208 populations in cores within the network and other marine records were explored using

209 statistical comparisons of their average geochemical signature and graphical comparisons on

210 bivariate plots. The similarity coefficient function (SC) of Borchardt et al. (1972) was utilised

211 to construct a matrix for all these comparisons (Table S13). Twenty-five of the comparisons

212 returned SC values greater than 0.97, which implies there are strong similarities in the

213 geochemical signatures and further assessment was required to determine if they are

214 correlatives. A combination of three main factors were used to rule out most of these

215 comparisons as potential correlatives; large stratigraphic discrepancies, subtle geochemical

216 differences, and occurrence at different depths in the same core sequence. Despite the

217 majority being ruled out, upon further assessment two of the comparisons with high SC

218 values were found to have very strong geochemical similarities and consistent stratigraphic

219 positions and are suggested as correlations between marine sequences in the network (see

220 Section 4).

221

222 *3.2 Assessing the isochronous nature of cryptotephra deposits*

223

224 Several of the deposits reported here have been described in Abbott et al. (submitted) as

225 illustrative examples for assessing the dominant controls on tephra deposition in the North

226 Atlantic region. We synthesise these results in a framework of tephra deposits that represent

227 isochronous marker horizons identified using protocols set out in Griggs et al. (2014) and

228 Abbott et al. (submitted). The key characteristics used to define isochronous horizons are: (i)

229 a clear peak in the shard concentration profile that can be used as the isochron position and

230 (ii) a homogenous geochemical population, indicative of material deriving from a single

231 volcanic eruption. The deposit type scheme outlined in Abbott et al. (submitted) is utilised to

232 assess deposits as it accounts for variability in geochemical signatures and shard

233 concentration profiles observed for North Atlantic marine tephra deposits. While Type 1 and

234 3 deposits are typically characterised by single homogenous populations there is greater

235 variability and complexity in the geochemical signatures of Type 2 deposits. For the latter a

236 larger number, up to 60 but typically >30, of single-grain major element analyses were

237   gained. These were graphically assessed to explore the relative homo/heterogeneity of

238   deposits, define homogenous populations that may have derived from single eruptions,

239   quantify their relative dominance within the deposits and categorise them as Type 2A or Type

240   2B deposits. Outliers were defined as analyses that were not consistently associated with a

241   defined population. For some deposits where populations were not defined all analyses could

242   be categorised as 'outliers', however, in these situations shards were grouped based on

243   affinities to the Icelandic rock suites.

244

245   *3.3 Age and stratigraphic constraints*

246

247   The timing of deposition for each tephra deposit is given based on the available

248   climatostratigraphy for the specific core within which the horizons were isolated (Table 1).

249   For some records, there is strong stratigraphic control based on proxy records from the cores

250   that record the DO events which characterised the North Atlantic region during the last

251   glacial period, e.g. MD04-2822 and MD04-2829CQ. However, for other cores, e.g. MD99-

252   2251 and GIK23415-9, the stratigraphic frameworks are not as distinct with deposits from the

253   Heinrich Events providing the best stratigraphic control. Due to uncertainties in the relative

254   timing of closely spaced horizons not identified in the same core sequence the stratigraphic

255   relationships presented in Figure 2 should be treated with caution, e.g. the cluster of horizons

256   that have been identified in various cores around the H4 event (Figure 2). Further

257   investigations of these horizons, such as their tracing into other sequences, may help to refine

258   the sequence of the volcanic events in the future.

259

260   **4. North Atlantic Tephra Framework**

261

262   An improved marine tephra framework for the North Atlantic between 25-60 kyr BP is

263   presented in Figure 2 and Table 1. Overall, a framework of 14 isochronous horizons can be

264   defined, including 8 new isochronous horizons presented for the first time, 3 cryptotephra

265   deposits identified in MD04-2820CQ by Abbott et al. (2016) and 3 previously published

266   deposits (NAAZ II, FMAZ IV and FMAZ II). This represents a significant increase in the

267   number of tephra marker horizons that could be utilised for the correlation of records during

268   this period.

269

270   With the exception of NAAZ II (II-RHY-1) and MD04-2820CQ 497-498 cm, all tephras in

271   the framework are basaltic in composition and originated from Iceland, specifically from the

272   Grímsvötn, Kverkfjöll, Hekla/Vatnafjöll and Katla volcanic systems (Table 1). The most

273   widespread isochronous horizon in the framework is the NAAZ II (II-RHY-1) (Figures 3 and

274   4). The wide distribution and importance of this horizon had been established in prior studies,

275   however, here we have isolated it in more sequences, gained greater control on the timing of

276   deposition, with peaks in shard concentration determined at a 1 cm resolution, and provided

277   an improved geochemical signature for the horizon (Section 4.1.1). The geographical range

278   of the previously identified FMAZ IV can be expanded, to a limited extent, from the Faroe

279   Islands region to the Norwegian Sea following its identification in MD95-2010 (Figure 5;

280   Section 4.1.2).

281

282   Within our network only two cores, MD04-2822 and MD04-2829CQ, exclusively preserved

283   isochronous Type 1 deposits (Figures 6a and 6b). New isochronous horizons were also

284   identified in two further cores, MD99-2251 and GIK23415-9, alongside other deposits

285   without clear isochronous characteristics, i.e. Type 2B and Type 4 deposits (Figures 7a and

286   8a), which can be attributed to temporal variability in the processes controlling tephra

287   deposition at these sites (see Abbott et al., submitted). Further details regarding all the

288   isochronous horizons are provided in Section 4.1 in chronological order from the oldest to the

289   youngest horizon.

290

291   The Type 2B and Type 4 horizons are not overlooked though as analysis showed that within

292   many of these deposits significant homogenous geochemical populations could be isolated

293   (Figures 7b and 8b; Table 1). These populations are presented alongside the framework of

294   isochronous horizons as their geochemical homogeneity suggests that they were derived from

295   single volcanic events, but, at present, questions remain over their depositional origin and

296   isochronous nature. Further investigations, however, may permit their integration into the

297   regional tephra framework and this is discussed further in Section 4.2.

298

299   *4.1 Isochronous Horizons*

300

301   *4.1.1 NAAZ II*

302

303   NAAZ II is a crucial deposit within the North Atlantic marine tephra framework and it has

304   been identified at nine sites within our network as a clear peak in rhyolitic material and at 6

305   sites basaltic/intermediate material was also present. Based on occurrences of NAAZ II in

306   several North Atlantic sites this ash zone was defined as being composed of five geochemical

307   populations, one rhyolitic (II-RHY-1) and four basaltic (II-THOL-1, II-THOL-2, II-THOL-3

308   and II-TAB-1) by Kvamme et al. (1989).

309

310   Shards from the peaks in rhyolitic material at the 9 sites have a consistent homogenous

311   transitional alkali rhyolitic composition (Figure 3ai and 4b; Table S2). In comparison to prior

312   characterisations of NAAZ II from several North Atlantic marine cores strong similarities can

313   be observed for some elements, e.g. FeO and CaO (Figure 3bi) but some offsets are apparent

314   for other elements, e.g. Na_2O and SiO_2 (Figure 3bii). These differences are reflected in

315   similarity coefficient comparisons (Table S2) and are consistent with sodium loss affecting

316   the older EPMA analyses, particularly for the analyses from Kvamme et al. (1989), and are

317   highly unlikely to indicate a different source for the material (Hunt and Hill, 1993; Kuehn et

318   al., 2011). Therefore, the nine deposits in this network can be correlated to the II-RHY-1

319   component of NAAZ II. These new analyses provide an up-to-date composition for this

320   component and highlight that data quality must be considered when assessing correlations

321   between datasets, especially for rhyolitic material.

322

323   A peak in brown shards was isolated in direct association with the II-RHY-1 peak at 6 sites

324   (Figure 4b; e.g. in MD99-2251 (Figure 4a)). Compositional analyses revealed a range of

325   signatures with basaltic and intermediate material present (Figure 3aii). Shards related to

326   three of the basaltic populations of Kvamme et al. (1989) have been identified, but no shards

327   related to the II-THOL-3 population were isolated (Figure 3c). Glass shards with an

328   intermediate trachyandesite to trachydacite composition have been identified (Figure 3aii)

329   and grouped as a new population, which we name II-INT-1. Some material with an

330   intermediate composition was found in association with the proximal Icelandic deposit

331   correlated to NAAZ II, the Thorsmörk ignimbrite (Jørgensen, 1980), however, this is less

332   evolved than the material in these marine deposits with SiO_2 values of 56-58 % and is

333   unlikely to be directly related. This additional intermediate population suggests that the

334   basaltic material associated with NAAZ II derives from more individual eruptions than

335   previously thought. This assertion is also supported by differences in the composition of

336   material from this study attributed to the populations of Kvamme et al. (1989) which may

337   indicate they grouped material from multiple eruptions as single populations. For example,

338   shards from M23485-1 and GIK23415-9 display geochemical differences, e.g. Figure 3cii,

339   despite all falling into the II-THOL-2 field of Kvamme et al. (1989). At three of the sites the

340   brown shards are related to a single population, homogenous populations within the II-

341   THOL-2 geochemical field in M23485-1 and JM11-19PC and only shards from the

342   intermediate population are present in MD01-2461 (Figure 4c). The remaining three sites

343   preserve a mix of populations. MD04-2820CQ preserves three populations (II-THOL-1, II-

344   THOL-2 and II-INT-1), each exceeding 24% of the shards present. GIK23415-9 and MD99-

345   2251 are dominated by the II-THOL-1 and II-TAB-1 populations respectively.

346

347   The contrast between the homogeneity of the rhyolitic material at all sites and the

348   heterogeneity and inconsistent signatures of the basaltic/intermediate material may indicate

349   that despite coeval deposition the two components were transported differentially. It has been

350   suggested that NAAZ II was primarily transported from Iceland via sea-ice rafting and

351   primary airfall (e.g. Ruddiman and Glover, 1972; Austin et al., 2004; Wastegård et al., 2006).

352   Sea-ice rafting may have contributed towards the relatively higher rhyolitic shard

353   concentrations at sites to the south and west of Iceland. The geochemical homogeneity and

354   distinct peak with an upward tail in rhyolitic shard concentrations (i.e. Type 3 deposits; e.g.

355   Figure 4ai), observed at all sites is consistent with these transport processes and supports the

356   isochronous nature of the II-RHY-1 component.

357

358   The heterogeneity of the basaltic material and relative discreteness of the concentration

359   peaks, e.g. Figure 4aii, is most consistent with transport via iceberg rafting and the between-

360   site contrasts in geochemical signatures highlights that icebergs calved from different

361   margins of the Icelandic ice sheet could have transported and deposited material at the core

362   sites. The absence of basaltic material associated with the rhyolitic peaks in the MD04-2822

363   and MD95-2010 sites is consistent with the findings of Abbott et al. (submitted) that ice

364   rafting did not transport tephra to these sites during the last glacial period. Transportation via

365   iceberg rafting can delay the deposition of tephra, therefore the peaks in basaltic material

366   related to NAAZ II should not be utilised as isochronous markers. It cannot be ruled out that

367   one or more of the basaltic populations were deposited coevally via primary airfall with the

368   rhyolitic material, particularly at sites only containing one population. However, it is unlikely

369   that this process deposited all of the basaltic populations with subsequent amalgamation in

370 the sediment column, as shard concentrations profiles for that type of deposit (Type 4)

371 typically have a greater spread within sequences and display multiple concentration peaks.

372

373 The coeval deposition of the two shard types may indicate that the volcanic eruption that

374 produced the rhyolitic tephra horizon triggered an ice-rafting event which deposited the

375 basaltic material, but the resolution of the marine records under investigation here is

376 insufficient to resolve this temporal phasing.

377

378 *4.1.2 FMAZ IV – MD95-2010 915-916 cm*

379

380 FMAZ IV was identified in the MD95-2010 core from the Norwegian Sea as a discrete

381 deposit at 915-916 cm depth (Figure 5a). This deposit has a homogenous basaltic

382 composition with affinities to the Icelandic tholeiitic rock suite and the products of the

383 Grímsvötn volcanic system. The composition of MD95-2010 915-916 cm is identical to the

384 characterisation of the JM11-19PC 542-543 cm deposit of Griggs et al. (2014) (Figure 5b; SC

385 – 0.985), previously correlated to the FMAZ IV of Wastegård and Rasmussen (2014).

386 According to the age model and stratigraphy for MD95-2010 from Dokken and Jansen (1999)

387 this layer has an age of ~44.45 ka BP and was deposited during the DO-12 event based on the

388 magnetic susceptibility record. This stratigraphic position and age estimate are consistent

389 with the work of Wastegård and Rasmussen (2014). This horizon has previously not been

390 identified outside the Faroe Islands region and, therefore, this discovery expands its

391 geographical range in a North easterly direction to the Nordic Sea.

392

393 *4.1.3 MD04-2820CQ 524-525 cm*

394

395 MD04-2820CQ 524-525 cm has previously been described by Abbott et al. (2016) where it

396 was identified as a clear peak in shard concentrations spanning ~6 cm depth. Geochemical

397 analyses of shards from this deposit form a homogenous tholeiitic basaltic population sourced

398 from either the Grímsvötn or Kverkfjöll Icelandic volcanic systems. These characteristics

399 allow the deposit to be defined as Type 2A and allied with a lack of direct covariance with

400 IRD this deposit is thought to have been deposited via primary airfall despite occurring

401 during a period of elevated IRD concentrations (Abbott et al., 2016).

402

403 *4.1.4 MD04-2822 2017-2018 cm*

High-resolution analysis of MD04-2822 showed a well-constrained peak in brown tephra shards in all grain-size fractions at 2017-2018 cm depth (Figure 6a). According to the core stratigraphy this horizon was deposited during a stadial period prior to the warming transition into DO-9 (Figure 6a). Shards have a homogenous basaltic composition with affinities to the Icelandic tholeiitic rock suite and the products of the Grímsvötn volcanic system (Figure 6c).

4.1.5 MD04-2820CQ 497-498 cm

MD04-2820CQ 497-498 cm was identified as a small peak in colourless shards during a period of consistently elevated concentrations (Abbott et al., 2016). Shards from the peak have a transitional alkali rhyolitic composition and form a single population with affinities to a number of distal tephra deposits previously attributed to the Katla volcanic system (Abbott et al., 2016). This horizon is notable as it is the only other rhyolitic horizon within the marine tephra framework apart from the rhyolitic component of NAAZ II (Table 1). Due to its homogeneity and the prevalence of shards in the 25-80 μm fraction this deposit was interpreted as an isochronous horizon deposited via primary airfall (Abbott et al., 2016).

4.1.6 MD04-2820CQ 487-488 cm

Deposited just prior to Heinrich Event 4, MD04-2820CQ 487-488 cm was identified as a clear peak in brown shard concentrations across all grain size fractions spread over ~3 cm depth (Abbott et al., 2016). While some transitional alkali outliers are present within shard analyses from this deposit the vast majority of shards (~85 %) form a homogenous geochemical population with a tholeiitic basaltic composition and affinities to the Grímsvötn volcanic system (Abbott et al., 2016). This homogenous composition and a lack of covariance of shard concentrations with IRD suggests it was not deposited via iceberg rafting. Deposition is likely to have occurred via primary airfall, however, the high proportion of shards in the coarser grain-size fractions (80-125 μm and >125 μm) in comparison to the 25-80 μm fraction may also indicate transport via sea-ice rafting. Neither process would impart a significant temporal delay and thus MD04-2820CQ 487-488 cm is viewed as an isochronous deposit (Abbott et al., 2016).

4.1.7 MD04-2829CQ 934-935 cm and 930-931 cm

438

439 Two distinct and closely spaced peaks in brown glass tephra shards were isolated in MD04-

440 2829CQ with concentrations of ~35 shards per 0.5 g dws in the 25-80 μm grain-size fraction

441 (Figure 6b). Only a limited number of shards were isolated in one of the three samples

442 between these peaks. The stratigraphy for MD04-2829CQ indicates that these horizons were

443 deposited during and just after the rapid warming into DO-8 (Figure 6b; Hall et al., 2011).

444 Shards from both peaks were geochemically analysed and this revealed two homogenous

445 basaltic populations with affinities to the Icelandic tholeiitic rock suite and the products of the

446 Grímsvötn volcanic system. However, there are distinct differences in Al_2O_3, FeO, CaO and

447 MgO between the two deposits (Figure 6c). These differences show that despite being

448 separated by only 3 cm of sediment the horizons were produced by two separate volcanic

449 eruptions and coupled with their other characteristics can be considered as valuable

450 isochronous marker horizons.

451

452 *4.1.8 MD04-2822 2004-2005 cm*

453

454 High-resolution shard counts identified brown shards within the 25-80 and >125 μm grain-

455 size fractions in the 2004-2005 cm sample of MD04-2822 (Figure 6a). While the shard

456 concentrations are low the peaks are discrete as no further shards were identified in adjacent

457 samples. According to the stratigraphy of the core this material was deposited shortly after

458 the warming transition into DO-8 (Figure 6a; Hibbert et al., 2010). Geochemical analysis

459 shows that shards from the deposit have a homogenous transitional alkali basaltic

460 composition (Figure 6c). The shards are characterised by high TiO_2 values of ~4.65 %wt and

461 comparisons to proximal Icelandic deposits demonstrate that the deposit was most likely

462 sourced from the Katla volcanic system (Figure 6c). The geochemical composition of the

463 material in this peak is very distinct from the material in the underlying MD04-2822 2017-

464 2018 cm horizon indicating that they represent two discrete events.

465

466 *4.1.9 MD99-2251 1680-1681 cm*

467

468 The highest brown shard concentrations in MD99-2251 were identified as a peak centred

469 around 1680-1681 cm depth (Figure 7a). Overall, high shard concentrations associated with

470 this peak cover approximately 10 cm depth, typical of a Type 2 deposit, and glass shards

471 from the main peak and a secondary peak at 1683-1684 cm were geochemically analysed.

472

473   Shards from 1680-1681 cm form a clear homogenous population, with 76 % of the analyses

474   in this population (Figure 7b). High TiO_2 concentrations in excess of 4.4 %wt strongly

475   indicates an origin from the Katla volcanic system (Figure 7b). Within the remaining 25 % of

476   shards a minor population (6 %) of tholeiitic material, most likely sourced from the

477   Kverkfjöll volcanic system, was also identified alongside several outlying shards (Figure 7b).

478   The significant dominance of a single homogenous population in the 1680-1681 cm peak,

479   suggests that this material was deposited via primary airfall and that this tephra deposit

480   represents an isochronous marker horizon despite being deposited during a period of elevated

481   IRD concentrations associated with Heinrich Event 3 (Figure 7a).

482

483   The geochemical signature of material from the underlying 1683-1684 cm peak is the same as

484   the major 1680-1681 cm peak suggesting that this does not represent an earlier and separate

485   depositional event but downward reworking of material from the main concentration peak.

486   The slight deviation of the shard concentration profile from a gradational downward tail

487   could imply that any reworking processes were not uniform across the core. Such variability

488   was observed by Griggs et al. (2015) in 3D reconstructions of the structure of tephra deposits

489   gained using X-ray microtomography.

490

491   *4.1.10 MD04-2829CQ 800-801 cm*

492

493   The highest shard concentrations in core MD04-2829CQ were identified at 800-801 cm, with

494   increases observed in all grain-size fractions (Figure 6b). This deposit is very distinct with

495   limited shards identified in adjacent samples. Stratigraphic constraints indicate that this

496   horizon was deposited in the cold period prior to DO-4 (Figure 6b; Hall et al., 2011).

497   Compositional analysis of individual shards shows that all material has a tholeiitic basaltic

498   composition and can be grouped into two homogenous populations, with clear bimodality

499   observed for some oxides, including TiO_2, FeO, CaO and MgO (Figure 6c). Analyses

500   grouped into population THOL-1 were only derived from shards from the 25-80 μm grain-

501   size fraction, whereas the majority of analyses in population THOL-2 are from shards >80

502   μm in diameter. Based on comparisons to proximal Icelandic deposits THOL-1 has a close

503   affinity to products of Grímsvötn while THOL-2 is most likely derived from the Kverkfjöll

504   volcanic system (Figure 6b). This implies that the deposit was formed from the deposition of

505   material from two coeval eruptions of these volcanic centres.

506

4.1.11 MD04-2822 1836-1837 cm - GIK23415-9 225-226 cm

508

Within the MD04-2822 record the largest peak in brown shards was identified at 1836-1837
cm depth with >40 shards per 0.5 g of dws present in the 25-80 μm fraction (Figure 6a). The
material is stratigraphically well constrained with only 2 shards present in the underlying
sample. According to the stratigraphy this material was deposited during the cold stadial
period shortly before the transition into DO-4 (Hibbert et al., 2010). Compositional analysis
shows that material from this peak has a transitional alkali basaltic composition and forms a
homogenous geochemical population (Figure 6c). Comparisons to proximal Icelandic
deposits indicate that the horizon was sourced from either the Katla or Hekla/Vatnafjöll
volcanic system (Figure 6c).

518

A discrete peak in shard concentrations, restricted to 1 cm and with the characteristics of a
Type 1 deposit, was also isolated between 225-226 cm in GIK23415-9 (Figure 8a).
Geochemical analysis of the shards from this deposit shows that all have a transitional alkali
composition (Figure 8b). Within the analyses bimodality can be observed for some elements,
most notably TiO_2, and they can be split into two homogenous populations. A dominant
population (TAB-1) of 70 % of the shards with low TiO_2 values and a smaller population
(TAB-2) of 15 % of the analysed shards with TiO_2 values ~0.35% wt higher. TiO_2 values
have been identified as one of the primary oxides that can be used to discriminate between
Icelandic basaltic eruptions from the last glacial period (e.g. Bourne et al., 2013, 2015). The
remaining 15 % of analyses are classified as outliers. Comparisons to proximal deposits show
that the populations have similarities to the products of both the Katla and Hekla/Vatnafjöll
volcanic systems (Figure 8b). GIK23415-9 225-226 cm was deposited during Heinrich Event
3 which could suggest it was deposited via iceberg rafting. However, the relative dominance
of the TAB-1 population and a lack of direct covariance of shard concentrations with IRD,
with the discrete tephra peak contrasting with elevated IRD concentrations for ~25 cm of core
depth, do not support this interpretation. These indicators provide support for primary airfall
deposition of tephra shards from either a single chemically bimodal eruption or two closely
timed events.

537

Statistical analysis (SC of 0.987) and graphical comparisons support a correlation between
MD04-2822 1836-1837 cm and GIK23415-9 225-226 cm (TAB-1) (Table S13; Figure 9a). In

16

540 addition, there is a consistency in the stratigraphic position of the two horizons. MD04-2822

541 1836-1837 cm was deposited between DO events 5 and 4 (Figure 6a), while GIK23415-9

542 225-226 cm was deposited at the end of Heinrich Event 3 (Figure 8a), which, based on a

543 comparison of ages for the Heinrich Events from Sanchez Goñi and Harrison (2010) and the

544 Greenland ice-core chronology presented in Seierstad et al. (2014), occurred after Greenland

545 Interstadial (GI) 5, the ice counterpart to DO-5. Based on the available information, we assert

546 that these two deposits are the products of the same volcanic event and form a tie-line

547 between the two relatively closely spaced sequences (Figure 2).

548

549 *4.1.12 GIK23415-9 173-174 cm*

550

551 A peak in basaltic glass shard concentrations was identified in the GIK23415-9 core at a

552 depth of 173-174 cm, following Heinrich Event 2 (Figure 8a). The shard concentration

553 profile of this deposit is akin to a Type 1 deposit with a relatively discrete peak in shard

554 concentrations restricted to ~1 cm (Figure 8a). Geochemical analysis of shards from this

555 deposit show one clear homogenous population, composed of 60 % of the analysed shards,

556 with a basaltic tholeiitic composition and an affinity to the Kverkfjöll volcanic system

557 (Figure 8b). The remaining 40 % are heterogeneous and can be regarded as outliers (Figure

558 S8). While the overall homogeneity of the deposit is not as distinct as most Type 1 deposits,

559 the occurrence of a very homogenous population deposited during a period of low IRD input

560 does suggest that airfall deposition occurred and it forms an isochronous deposit. The

561 outlying shards may derive from a low background of IRD input of ice-rafted shards during

562 this period. In addition, the use of the percentage abundance of populations to assess this

563 deposit has some limitations as only a low number of analyses, 15, were gained from shards

564 within this deposit.

565

566 *4.2 Significant Geochemical Populations and Possible Isochrons*

567

568 In addition to the isochronous deposits outlined in Section 4.1 six tephra deposits in the

569 MD99-2251 core and four in the GIK23415-9 sequence were assessed as having non-

570 isochronous characteristics and have been classified as Type 2B or Type 4 deposits (Figures

571 7a and 8a). The main criterion underpinning this assessment was the geochemical

572 heterogeneity of the deposits, indicative of the amalgamation of material from a number of

573 volcanic eruptions. However, while only three deposits, MD99-2251 1654-1655 cm and

17

574   1796-1797 cm and GIK23415-9 193-194 cm, have fully heterogenous compositions the other

575   deposits contain 16 significant homogenous geochemical populations, in total, within their

576   overall heterogeneity (Figure 2; Table 1). The significant geochemical populations may relate

577   to single volcanic eruptions, but due to their occurrence within heterogenous deposits further

578   investigations are required to determine if they were deposited isochronously. The full

579   geochemical signatures of all MD99-2251 and GIK23415-9 deposits and the populations

580   identified within them are summarised in Figures S1-S14 and Tables S8 and S10.

581

582   The 16 populations all have a basaltic composition and were sourced from Iceland. In

583   addition to the volcanic regions which deposited isochronous horizons in the North Atlantic

584   region, i.e. Grímsvötn, Kverkfjöll, Hekla/Vatnafjöll and Katla, homogenous populations with

585   geochemical similarities to the products of the Veidivötn-Bardarbunga and Vestmannaeyjar

586   volcanic systems were identified (Table 1; Figures 7a and 7b). Their relative dominance

587   within the deposits is variable, ranging from ~10 to 60 % of the total single-shard analyses

588   used to characterise the deposits (Tables S8 and S10).

589

590   Co-variance of shard concentration profiles with IRD records was another variable used to

591   assess the isochronous nature of the deposits (Abbott et al., submitted). Some of the deposits

592   with heterogenous signatures were deposited during periods of elevated or rising IRD

593   concentration, which could indicate transport via iceberg rafting and a significant temporal

594   delay between eruption and deposition. However, iceberg rafting is not the only process that

595   can amalgamate the products of multiple eruptions. For example, for some deposits post-

596   depositional mixing in the sediment column of the products of several closely-timed

597   eruptions cannot be ruled out as some were isolated within periods of limited IRD deposition.

598   In this later scenario deposition would have been via primary airfall with no temporal delay,

599   however, determining the isochron position could be challenging as complexity is often

600   observed in the shard concentration profiles. Primary airfall deposition could also have

601   occurred during a period of ice-rafting deposition resulting in the incorporation of a

602   homogenous population within a heterogenous background signal.

603

604   These differing scenarios and the uncertainty in the depositional processes implies that

605   further investigations are required to assess whether these populations are isochronous. As

606   such, we report the significant geochemical populations, but do not incorporate them within

607   the regional tephra framework until further evidence is gained. The latter may include their

608   identification in other North Atlantic marine cores and/or the Greenland ice-core tephra

609   framework in a similar stratigraphic position. In addition, for some records the covariance

610   with IRD could not be fully explored due to the lower resolution in this dataset relative to the

611   shard concentration profiles. Improved high-resolution IRD records would be highly

612   advantageous for further assessing depositional processes. An example of how tracing these

613   populations into other records could provide further insights into their isochronous nature is

614   provided within our work.

615

616   The assessment of potential correlations (Table S13), highlighted a strong similarity between

617   the geochemical signature of FMAZ II and the THOL-1 population in the GIK23415-9 202-

618   203 cm deposit (Figure 7; Table 1). The SC comparison returned a high coefficient of 0.990,

619   demonstrating that the signatures were nearly identical, and this observation is corroborated

620   by graphical comparisons (Figure 9b). Stratigraphically, FMAZ II has been identified

621   between Heinrich Events 3 and 2 in marine records and was deposited prior to an increase in

622   IRD concentrations in the ENAM93-21 core (Rasmussen et al., 2003) and after GI-3 in the

623   Greenland ice-core stratigraphy (Davies et al., 2010). GIK23415-9 202-203 cm was deposited

624   during a period of increasing IRD concentrations related to the start of Heinrich Event 2

625   (Figure 8a). These stratigraphic positions are consistent and coupled with the strong

626   geochemical similarities could imply isochronous deposition from the same volcanic event.

627   GIK23415-9 202-203 cm (THOL-1) is one of 4 homogenous geochemical populations within

628   the deposit and, due to their co-occurrence, it was interpreted as being deposited via iceberg

629   rafting. The proposed correlation does not contradict this interpretation but could demonstrate

630   that GIK23415-9 202-203 cm (THOL-1) was deposited via airfall during a period when

631   tephra from other events was rafted by icebergs. Overall, this further highlights the

632   complexity of some deposits, but demonstrates how these significant geochemical

633   populations are important to consider as potential isochronous markers.

634

635   *5. Discussion*

636

637   *5.1 Future application of the North Atlantic Marine Tephra Framework*

638

639   The North Atlantic marine tephra framework between MIS 2-3 has been significantly

640   improved through the most extensive application of cryptotephra methods, comprehensive

641   compositional analysis and rigorous protocols to assess the isochronous nature of each

642   deposit. For a long period only a limited number of horizons had been identified in this time

643   period (Haflidason et al., 2000; Wastegård et al., 2006). Now this framework includes 14

644   isochronous horizons that have considerable promise for correlating and synchronising

645   palaeoclimatic records. There is also potential to add further isochronous markers given the

646   significant geochemical populations identified in heterogenous deposits also reported in this

647   study.

648

649   NAAZ II remains a dominant tephra within this framework and our work has identified it in

650   numerous additional cores with greater control on the timing of deposition derived from high-

651   resolution shard counts and an improved geochemical signature for the widespread rhyolitic

652   component (II-RHY-1). This tephra represents a key marker horizon for the period providing

653   an isochronous tie-line linking numerous widespread marine cores and the Greenland ice-

654   core records beyond the radiocarbon window. The distribution of the FMAZ IV has been

655   extended from the Faroe Islands region into the Nordic Seas and has the potential to be a key

656   tie-line for DO 12. However, despite being found previously in several North Atlantic cores

657   and the NGRIP ice-core (see summary map in Davies et al., 2012) the FMAZ II was only

658   found in one additional core, GIK23415-9. Furthermore, most of the new cryptotephras are

659   single-core occurrences, highlighting challenges with cryptotephra tracing within the North

660   Atlantic Ocean. The limited tracing of horizons may reflect the difficulties of detecting and

661   isolating deposits that often only contain a low concentration of shards, but could also

662   indicate the relatively constrained dispersal of the basaltic eruptions depositing material over

663   the North Atlantic. Only one correlation has been made between newly identified

664   isochronous horizons in the framework, MD04-2822 1836-1837 cm and GIK23415-9 225-

665   226 cm (Section 4.1.11; Figure 2). These cores are relatively closely spaced, supporting the

666   suggestion of limited basaltic ash dispersal.

667

668   Assessing potential correlations between the records highlighted that while a range of factors

669   demonstrated that there are few direct correlations, many of the horizons have similar

670   geochemical signatures, especially eruptions from the Grímsvötn and Katla volcanic systems

671   (Table 1). This corroborates the findings of Bourne et al. (2015) who observed similar

672   repetition of geochemical signatures from these systems in tephra horizons in the Greenland

673   ice-cores. The repetition of geochemical signatures is particularly notable for the period

674   around H4 as a cluster of six closely spaced horizons has been identified in the marine cores

675   (Figure 2). Of these, five horizons have similar tholeiitic basaltic compositions and are

676   thought to be derived from the Grímsvötn volcanic system, however, subtle differences in

677   geochemical signatures show they represent individual events.

678

679   The observations that the new cryptotephras in the North Atlantic region may have limited

680   dispersal and geochemical similarities do provide challenges for future correlation. There is,

681   however, the potential to constraint a number of rapid climate events, such as H4 and DO 8

682   and H3 as clusters of isochronous horizons are present around those events. Further

683   investigations should initially focus on sites close to those preserving the isochronous

684   horizons in this framework and/or re-evaluate previously explored sites (e.g. green sites on

685   Figure 1), with adaptions to the methodological approach discussed in Section 5.3. It is

686   imperative that potential correlations are rigorously assessed as correlating horizons or

687   populations with close, but not identical, geochemical signatures, could lead to the

688   establishment of incorrect tie-lines being defined between records. Other supporting evidence

689   such as broad stratigraphic constraints and independent age estimates can also be used to

690   support these correlations. A detailed assessment of possible correlations to the Greenland

691   ice-cores will be discussed in a forthcoming publication whereby trace element signatures are

692   also employed to assess and support correlations.

693

694   *5.2 Reconstructing Icelandic Volcanic History*

695

696   This framework adds to our understanding of the volcanic history of Iceland during the last

697   glacial period between 25-60 kyr BP. The dominance of basaltic over rhyolitic horizons and

698   the high productivity of the Grímsvötn/Kverkfjöll and Katla volcanic systems around

699   Heinrich Event 4 and Henrich Event 3 respectively, is consistent with the Greenland ice-core

700   tephra framework for the same period (Bourne et al., 2015). Basaltic horizons potentially

701   sourced from other volcanic centres were observed, including the Veidivötn-Bardabunga and

702   Vestmannaeyjar volcanic systems. There are very few or no tephras in the Greenland

703   framework with geochemical similarities to those horizons, potentially due to a bias in

704   dispersal direction and/or a low number of eruptions from these sources. This observation

705   shows that a more complete reconstruction of Icelandic volcanism will be gained by

706   integrating the two frameworks. There is, however, a notable difference between the number

707   of tephra deposits identified between the marine and ice-core records. With 99 volcanic

708   events recorded in the Greenland records in contrast to 33 events in the marine archives, if

709   the homogenous populations are assumed to derive from individual volcanic events. The

710 lower resolution of the marine records, the potential for the amalgamation of airfall deposits
711 and post-depositional reworking processes are the most likely causes of this disparity.

712

713 *5.3 Improving the Marine Tephra Framework*

714

715 This work has demonstrated the potential of identifying isochronous cryptotephras in North
716 Atlantic marine records of the last glacial period. However, the methodology employed to
717 identify cryptotephras in this work most likely created a bias towards the identification of
718 horizons depositing a high concentration of tephra shards at core sites. As discussed by
719 Timms et al. (2017) the process of completing low-resolution scans prior to a subjective peak
720 selection for high-resolution (1 cm) analysis may introduce a bias as low concentration or
721 discrete peaks might not have sufficient shard concentrations to be observed in the low-
722 resolution record. The background of tephra that is prevalent at some marine sites could mask
723 individual eruptions that deposited a low concentration of shards. In the ice-core records
724 tephra events have been defined on the basis of as few as 3 shards (Bourne et al., 2015).
725 Detecting deposits of this kind would be particularly challenging in the marine environment
726 as they could be dismissed as "background" concentrations or hidden with the upward or
727 downward tail of a deposit or within an ash-rich deposit. We have attempted to explore the
728 presence of such horizons in this study but agree with Timms et al. (2017) who advocate the
729 use of more high-resolution shard concentration and chemical analyses to improve
730 tephrostratigraphies, while acknowledging that this may be limited by sediment availability,
731 time and financial considerations.

732

733 As such, the marine tephra framework presented in this study should not be viewed as
734 complete. However, by focusing on maximising the number and geographical range of
735 sequences an initial framework has been produced that is a significant step towards the
736 tephra-based synchronisation of North Atlantic marine records. Coupling the success of the
737 methodology, the initial framework presented here and the insights into the spatial controls
738 on tephra deposition discussed in Abbott et al. (submitted) there is huge potential to add to
739 and refine the marine tephra framework. This can be achieved through focusing on new cores
740 from areas with a high potential to preserve isochronous horizons and reassessing previously
741 investigated cores at a high-resolution over key intervals during which isochronous horizons
742 were identified in this work. In addition, innovative techniques for the identification and
743 quantification of tephra that are currently being developed, for example X-ray florescence

744   core scanning (e.g. Kolling and Bauch, 2017), hyperspectral core imaging (e.g. Aymerich et

745   al., 2016) and automated flow cytometry and microscopy (e.g. D'Anjou et al., 2014), could

746   be tested and incorporated into the methodological approach if appropriate.

747

748   *6. Conclusions*

749

750   A consistent methodology for the identification and characterisation of marine cryptotephras

751   and the rigorous assessment of the influence of transportation and deposition processes on

752   tephra deposits was used to build a North Atlantic marine tephra framework. Eleven

753   isochronous deposits were identified in a wide network of marine sequences and have been

754   integrated with prior data to create a marine tephra framework for the MIS 2-3 period. Key

755   information for each deposit such as their spatial extent, geochemical signature, eruptive

756   source and timing of deposition is synthesised. A number of significant geochemical

757   populations are also reported that require further work to assess whether they originate from

758   single volcanic eruptions and were deposited isochronously via primary airfall.

759

760   There is considerable potential to improve this framework by tracing the deposits into other

761   marine sequences or the identification of new deposits. Combining this framework with

762   knowledge of the processes controlling the deposition of tephra in the North Atlantic and the

763   identification of key areas where isochronous horizons are preserved provided in Abbott et al.

764   (submitted) these future investigations could be highly focussed, both temporally and

765   spatially. The full potential of this framework will only be realised if attempts are made to

766   trace these horizons into other archives such as the Greenland ice-cores and terrestrial

767   records. If successful they can act as time-synchronous tie-lines to correlate and synchronise

768   these palaeoclimatic records, providing insights into the phasing, rate, timing and

769   mechanisms forcing the rapid climate changes that characterised this period.

770

Figures

Figure 1: Location map of cores within the marine network (red) and other cores referred to in the text (green). Location (1) includes cores SO82-2, SO82-5, LO09-23, LO09-21, SO82-7 and SO82-4 described in Lackschewitz and Wallrabe-Adams (1997). Location (2) includes cores ENAM93-21 and ENAM93-20 and location (3) includes cores LINK16, LINK17, LINK15 and LINK04 described in Rasmussen et al. (2003), Wastegård et al. (2006) and Wastegård and Rasmussen (2014).

Figure 2: Schematic representation of the improved marine tephra framework for the North Atlantic between 25-60 kyr BP. Ages and the stratigraphic relationship of tephra horizons between cores are approximate should be treated with caution, see text for details. The ages utilised are based on either existing age models for sequences or estimates based on stratigraphic positions. Heinrich Events 2-5 are included as stratigraphic markers and their ages are based on those given in Sanchez Goñi and Harrison (2010).

Figure 3: (a) Total alkali v silica plot focusing on (i) rhyolitic material and (ii) basaltic and intermediate composition material from NAAZ II deposits in the marine network. (b) Comparison of new characterisations of NAAZ II rhyolitic material to characterisations from prior studies. Geochemical fields based on deposits in cores V23-23, V27-114, V23-82, V23-81 and V23-42 (Kvamme et al., 1989), MD95-2006 (Austin et al., 2004), ENAM93-20, ENAM33 and EW9302-2JPC (Wastegård et al., 2006) and MD99-2289 (Brendryen et al., 2011). (c) Comparison of basaltic material from newly characterised NAAZ II deposits to basaltic NAAZ II populations defined by Kvamme et al. (1989).

Figure 4: (a) Tephrostratigraphy of MD99-2251 between 1950-2030 cm covering the depth interval of NAAZ II. **(**i) Rhyolitic shards in the 25-80 μm grain-size fraction. (ii) Basaltic shards in the 25-80 μm grain-size fraction. (b) Peak concentrations of colourless (rhyolitic) and brown (basaltic) glass tephra shards in tephra deposits related to North Atlantic Ash Zone II. (c) Relative proportion of geochemical populations within analyses of basaltic glass tephra shards from NAAZ II deposits at six sites within the marine core network. Shard analyses not linked to the previously published populations or II-INT-1 were classified as uncorrelated.

822   **Figure 5:** (a) High-resolution concentration profiles of brown glass tephra shards between

823   910-920 cm in MD95-2010. (b) Comparison of the composition of MD95-2010 915-916 cm

824   to the characterisation of FMAZ IV (JM11-19PC 542-543 cm) from Griggs et al. (2014).

825

826   **Figure 6:** (a) (i) Percentage abundance of *Neogloboquadrina pachyderma* (sinistral) and (ii)

827   brown glass tephra shard tephrostratigraphy incorporating 5 cm and 1 cm counts for the

828   MD04-2822 core. (b) (i) Percentage abundance of *Neogloboquadrina pachyderma* (sinistral)

829   and (ii) brown glass tephra shard tephrostratigraphy incorporating 5 cm and 1 cm counts for

830   the MD04-2829CQ core. Foram abundances and Dansgaard-Oeschger event numbering for

831   MD04-2822 and MD04-2829CQ from Hibbert et al. (2010) and Hall et al. (2011)

832   respectively. (c) Geochemical characterisations of Type 1 tephra deposits in the MD04-2822

833   and MD04-2829CQ cores. (i) inset of total alkali vs. silica plot. Division line to separate

834   alkaline and sub-alkaline material from MacDonald and Katsura (1964). Chemical

835   classification and nomenclature after Le Maitre et al. (1989). (ii) FeO/TiO_2 vs. SiO_2 and (iii)

836   TiO_2 vs. Al_2O_3 compositional variations diagrams comparing the composition of MD04-2822

837   and MD04-2829CQ deposits to characterisations of proximal Icelandic material.

838   Geochemical fields for Icelandic source volcanoes are based on those utilised in Bourne et al.

839   (2015) and references within.

840

841   **Figure 7:** (a) (i) Percentage abundance of *Neogloboquadrina pachyderma* (sinistral), (ii) ash

842   free IRD concentration and (iii) tephrostratigraphic record of the MD99-2251 marine core.

843   Shard counts have been truncated for clarity. Shard counts in the 1686-1687 cm sample (*)

844   are 4991, 1862 and 507 shards per 0.5 g dws in the 25-80, 80-125 and >125 μm grain-size

845   fractions respectively. The shard counts for the 25-80 μm grain-size fraction from the 1904-

846   1905 cm sample (**) are 3776 shards per 0.5 g dws. Red bars denote samples depths from

847   which glass shards were subsequently extracted for compositional characterisation. (b)

848   Composition of significant geochemical populations identified in tephra deposits within the

849   MD99-2251 core. (i) inset of total alkali vs. silica plot. Division line to separate alkaline and

850   sub-alkaline material from MacDonald and Katsura (1964). Chemical classification and

851   nomenclature after Le Maitre et al. (1989). (ii) FeO/TiO_2 vs. SiO_2 and (iii) TiO_2 vs. Al_2O_3

852   compositional variations diagrams comparing significant geochemical populations from the

853   MD99-2251 deposits to characterisations of proximal Icelandic material. Geochemical fields

854   for Icelandic source volcanoes are based on those utilised in Bourne et al. (2015) and

855   references within.

26

856

Figure 8: (a) (i) Percentage abundance of *Neogloboquadrina pachyderma* (sinistral), (ii)
percentage IRD (>150 μm fraction) and (iii) tephrostratigraphic record of the GIK23415-9
marine core. *Np*(s) and IRD data from Vogelsang et al. (2004) and Weinelt (2004)
respectively. Labels for Heinrich Events from Weinelt et al. (2003) and Lu et al. (2007).
Shard counts have been truncated for clarity. Shard counts in the 193-194 cm sample are
5131 and 280 shards per 0.5 g dws in the 25-80 and >125 μm grain-size fractions
respectively. Red bars denote samples depths from which glass shards were subsequently
extracted for compositional characterisation. (b) Composition of significant geochemical
populations identified in tephra deposits within the GIK23415-9 core. (i) inset of total alkali
vs. silica plot. Division line to separate alkaline and sub-alkaline material from MacDonald
and Katsura (1964). Chemical classification and nomenclature after Le Maitre et al. (1989).
(ii) FeO/TiO_2 vs. SiO_2 and (iii) TiO_2 vs. Al_2O_3 compositional variations diagrams comparing
significant geochemical populations from the GIK23415-9 deposits to characterisations of
proximal Icelandic material. Geochemical fields for Icelandic source volcanoes are based on
those utilised in Bourne et al. (2015) and references within.

872

Figure 9: (a) Comparison of the MD04-2822 1836-1837 cm tephra horizon and the
GIK23415-9 225-226 cm (TAB-2) geochemical population. (b) Comparison of the FMAZ II
tephra horizon (JM11-19PC 202-203 cm from Griggs et al. (2014)) and the GIK23415-9 202-
203 cm (THOL-1) geochemical population.

Supplementary Information

Supplementary Figures

Figures S1-S13: Graphical analysis of geochemical populations identified within single-shard major element analyses from tephra deposits within the MD99-2251 (S1-S7) and GIK23415-9 (S8-S13) cores.

Supplementary Data

Table S1: Major oxide concentrations of shards from deposits related to the rhyolitic component of North Atlantic Ash Zone II (II-RHY-1). Deposits analysed are (i) MD04-2822 2168-2169 cm (ii) MD95-2024 1445-1446 cm (iii) MD99-2251 1974-1975 cm (supplementary peak) (iv) MD99-2251 2014-2015 cm (main peak) (v) M23485-1 622-623 cm (vi) GIK23415-9 429-430 cm (vii) MD01-2461 942-943 cm (supplementary peak) (viii) MD01-2461 947-948 cm (main peak) (ix) MD04-2820CQ 610-611 cm (x) JM11-19PC 618-623 cm (xi) MD95-2010 996-1000 cm.

Table S2: Similarity coefficient comparisons of average concentrations of analyses of the II-RHY-1 component in deposits from cores analysed within this work and by Kvamme et al. (1989), Austin et al. (2004), Wastegård et al. (2006) and Brendryen et al. (2011).

Table S3: Major oxide concentrations of shards from basaltic and intermediate shards directly associated with deposits of the rhyolitic component of North Atlantic Ash Zone II (II-RHY-1). Deposits analysed are (i) MD99-2251 2014-2015 cm (ii) M23485-1 622-623 cm (iii) GIK23415-9 429-430 cm (iv) MD01-2461 947-948 cm (v) MD04-2820CQ 610-611 cm (vi) JM11-19PC 618-623 cm.

Table S4: Major oxide concentrations of shards from the MD95-2010 915-916 cm tephra deposit.

Table S5: Major oxide concentrations of shards from tephra deposits in the MD04-2822 core. Deposits analysed are from the depths of (i) 1836-1837 cm (ii) 2004-2005 cm and (iii) 2017-2018 cm.

Table S6: Major oxide concentrations of shards from tephra deposits in the MD04-2829CQ core. Deposits analysed are from the depths of (i) 800-801 cm (ii) 930-931 cm and (iii) 934-935 cm.

Table S7: Major oxide concentrations of shards from tephra deposits in the MD04-2820CQ core. Deposits analysed are from the depths of (i) 487-488 cm (ii) 497-498 cm and (iii) 524-525 cm.

Table S8: Major oxide concentrations of shards from tephra deposits in the MD99-2251 core. Deposits analysed are from the depths of (i) 1654-1655 cm (ii) 1680-1681 cm (iii) 1683-1684 cm (iv) 1713-1714 cm (v) 1772-1773 cm (vi) 1796-1797 cm (vii) 1812-1813 cm and (viii) 1904-1905 cm.

Table S9: Analysis of geochemical populations present within tephra deposits identified in the MD99-2251 marine core. n = total number of analyses from deposits. Veid.-Bárd. = Veidivötn-Bárdarbunga.

Table S10: Major oxide concentrations of shards from tephra deposits in the GIK23415-9 core. Deposits analysed are from the depths of (i) 173-174 cm (ii) 193-194 cm (iii) 202-203 cm (iv) 225-226 cm (v) 302-303 cm (vi) 305-306 cm and (vii) 375-376 cm.

Table S11: Analysis of geochemical populations present within tephra deposits identified in the GIK23415-9 marine core. n = total number of analyses from deposits. Veid.-Bárd. = Veidivötn-Bárdarbunga.

Table S12a: Secondary standard analyses of the BCR2g standard made throughout analytical periods during which sample analyses presented in this work were analysed.

Table S12b: Secondary standard analyses of the Lipari standard made throughout analytical periods during which sample analyses presented in this work were analysed.

Table S13: Similarity coefficient comparisons between the geochemical signatures of isochronous horizons and significant geochemical populations in the marine tephra

945   framework for the North Atlantic between 25-60 ka BP. Method of Borchardt et al. (1972)

946   utilised. Red text shows SC values between 0.97 and 0.999 grey text shows SC values less

947   than 0.95.

References

Abbott, P.M., Bourne, A.J., Purcell, C.S., Davies, S.M., Scourse, J.D., Pearce, N.J.G., 2016. Last Glacial Period Cryptotephra Events in an Eastern North Atlantic Ocean Marine Sequence: Exploring Linkages to the Greenland Ice-Cores. Quaternary Geochronology 31, 62-76.

Abbott, P.M., Austin, W.E.N., Davies, S.M., Pearce, N.J.G., Hibbert, F.D., 2013. Cryptotephrochronology of a North East Atlantic marine sequence over Termination II, the Eemian and the last interglacial-glacial transition. Journal of Quaternary Science 28, 501-514.

Abbott, P.M., Austin, W.E.N., Davies, S.M., Pearce, N.J.G., Rasmussen, T.L., Wastegård, S., Brendryen, J., 2014. Re-evaluation and extension of the MIS 5 tephrostratigraphy of the Faroe Islands Region: the cryptotephras record. Palaeogeography, Palaeoclimatology, Palaeoecology 409, 153-168.

Abbott, P.M., Davies, S.M., 2012. Volcanism and the Greenland ice-cores: the tephra record. Earth-Science Reviews 115, 173-191.

Abbott, P.M., Davies, S.M., Austin, W.E.N., Pearce, N.J.G., Hibbert, F.D., 2011. Identification of cryptotephra horizons in a North East Atlantic marine record spanning marine isotope stages 4 and 5a (~60,000-82,000 a b2k). Quaternary International 246, 177-189.

Abbott, P.M., Griggs, A.J., Bourne, A.J., Davies, S.M., submitted. Tracing marine cryptotephras in the North Atlantic during the Last Glacial Period: Identification, characterisation and depositional controls. Submitted to Quaternary Science Reviews.

Austin, W.E.N., Abbott, P.M., 2010. Comment: Were last glacial climate events simultaneous between Greenland and France? A quantitative comparison using non-tuned chronologies. M. Blaauw, B. Wohlfarth, J.A. Christen, L. Ampel, D. Veres, K. Hughen, F. Preusser and A. Svensson (2009). Journal of Quaternary Science 25, 1045-1046.

Austin W.E.N., Wilson L.J., Hunt J.B., 2004. The age and chronostratigraphical significance of North Atlantic Ash Zone II. Journal of Quaternary Science 19, 137-146.

Aymerich, I.F., Oliva, M., Giralt, S., Martin-Herrero, 2016. Detection of Tephra Layers in Antarctic Sediment cores with Hyperspectral Imaging. PLoS ONE 11(1): e0146578. doi:10.1371/ journal.pone.0146578.

Blockley, S.P.E., Bourne, A.J., Brauer, A., Davies, S.M., Hardiman, M., Harding, P.R., Lane, C.S., MacLeod, A., Matthews, I.P., Pyne-O'Donnell, S.D.F., Rasmussen, S.O., Wulf, S., Zanchetta, G., 2014. Tephrochronology and the extended intimate (integration of ice-core, marine and terrestrial records) event stratigraphy 8-128 ka b2k. Quaternary Science Reviews 106, 88-100.

Bond, G., Broecker, W., Johnsen, S., McManus, J., Labeyrie, L., Jouzel, J., Bonani, G., 1993. Correlations between climate records from North Atlantic sediments and Greenland ice. Nature 365, 143-147.

998 Borchardt, G.A., Aruscavage, P.J., Millard, H., 1972. Correlation of the Bishop ash, a
999 Pleistocene marker bed, using instrumental neutron activation analysis. Journal of
1000 Sedimentary Petrology 42, 201-206.
1001
1002 Bourne, A.J., Davies, S.M., Abbott, P.M., Rasmussen, S.O., Steffensen, J.P., Svensson, A.,
1003 2013. Revisiting the Faroe Marine Ash Zone III in two Greenland ice cores: implications for
1004 marine-ice correlations. Journal of Quaternary Science 28, 641-646.
1005
1006 Bourne, A.J., Cook, E., Abbott, P.M., Seierstad, I.K., Steffensen, J.P., Svensson, A., Fischer,
1007 H., Schupbach, S., Davies, S.M., 2015. A tephra lattice for Greenland and a reconstruction of
1008 volcanic events spanning 25-45 ka b2k. Quaternary Science Reviews 118, 122-141.
1009
1010 Bramlette M.N., Bradley W.H., 1941. Geology and biology of North Atlantic deep-sea cores
1011 between Newfoundland and Ireland: I. Lithology and geologic interpretation. U.S. Geological
1012 Survey Professional Paper 196-A, 1-34.
1013
1014 Brendryen, J., Haflidason, H., Sejrup, H.P., 2010. Norwegian Sea tephrostratigraphy of
1015 marine isotope stages 4 and 5: Prospects and problems for tephrochronology in the North
1016 Atlantic region. Quaternary Science Reviews 29, 847-864.
1017
1018 Brendryen, J., Haflidason, H., Sejrup, H.P., 2011. Non-synchronous deposition of North
1019 Atlantic Ash Zone II in Greenland ice cores, and North Atlantic and Norwegian Sea
1020 sediments: an example of complex glacial-stage tephra transport. Journal of Quaternary
1021 Science 26, 739-745.
1022
1023 D'Anjou, R.M., Balascio, N.L., Bradley, R.S., 2014. Locating cryptotephra in lake sediments
1024 using fluid imaging technology. Journal of Paleolimnology 52, 257-264.
1025
1026 Davies, S.M., 2015. Cryptotephras: the revolution in correlation and precision dating. Journal
1027 of Quaternary Science 30, 114-130.
1028
1029 Davies, S.M., Abbott, P.M., Meara, Rh. H., Pearce, N.J.G., Austin, W.E.N., Chapman, M. R.,
1030 Svensson, A., Bigler, M., Rasmussen, T.L., Rasmussen, S.O., Farmer, E.J., 2014. A North
1031 Atlantic tephrostratigraphical framework for 130-60 ka b2k: new tephra discoveries, marine-
1032 based correlations, and future challenges. Quaternary Science Reviews 106, 101-121.
1033
1034 Davies, S.M., Abbott, P.M., Pearce, N.J.G., Wastegård, S., Blockley, S.P.E., 2012.
1035 Integrating the INTIMATE records using tephrochronology: rising to the challenge.
1036 Quaternary Science Reviews 36, 11-27.
1037
1038 Davies, S.M., Wastegård, S., Abbott, P.M., Barbante, C., Bigler, M., Johnsen, S.J.,
1039 Rasmussen, T.L., Steffensen, J.P., Svensson, A., 2010. Tracing volcanic events in the NGRIP
1040 ice-core and synchronising North Atlantic marine records during the last glacial period. Earth
1041 and Planetary Science Letters 294, 69-79.
1042
1043 Davies, S.M., Wastegård, S., Rasmussen, T.L., Svensson, A., Johnsen, S.J., Steffensen, J.P.,
1044 Andersen, K.K., 2008. Identification of the Fugloyarbanki tephra in the NGRIP ice core: a
1045 key tie-point for marine and ice-core sequences during the last glacial period. Journal of
1046 Quaternary Science 23, 409-414.
1047

1048 Dokken, T.M., Jansen, E., 1999. Rapid changes in the mechanism of ocean convection during
1049 the last glacial period. Nature 401, 458-461.
1050
1051 Griggs, A.J., Davies, S.M., Abbott, P.M., Coleman, M., Palmer, A.P., Rasmussen, T.L.,
1052 Johnston, R., 2015. Visualising tephra sedimentation processes in the marine environment:
1053 the potential of X-ray microtomography. Geochemistry, Geophysics, Geosystems 16, doi:
1054 10.1002/2015GC006073.
1055
1056 Griggs, A.J., Davies, S.M., Abbott, P.M., Rasmussen, T.L., Palmer, A.P., 2014. Optimising
1057 the use of marine tephrochronology in the North Atlantic: A detailed investigation of the
1058 Faroe Marine Ash Zones II, III and IV. Quaternary Science Reviews 106, 122-139.
1059
1060 Grönvold K., Óskarsson N., Johnsen S.J., Clausen H.B., Hammer C.U., Bond G., Bard E.,
1061 1995. Ash layers from Iceland in the Greenland GRIP ice core correlated with oceanic and
1062 land sediments. Earth and Planetary Science Letters 135, 149-155.
1063
1064 Gudmundsdóttir, E.R., Larsen, G., Björck, S., Ingólfsson, Ó., Striberger, J., 2016. A new
1065 high-resolution tephra stratigraphy in eastern Iceland: Improving the Icelandic and North
1066 Atlantic tephrochronology. Quaternary Science Reviews 150, 234-249.
1067
1068 Haflidason H., Eiriksson J., Van Kreveld S., 2000. The tephrochronology of Iceland and the
1069 North Atlantic region during the Middle and Late Quaternary: a review. Journal of
1070 Quaternary Science 15, 3-22.
1071
1072 Hall, I.R., Colmenero-Hidalgo, E., Zahn, R., Peck, V.L., Hemming, S.R., 2011. Centennial-
1073 to millennial-scale ice-ocean interactions in the subpolar northeast Atlantic 18-41 kyr ago.
1074 Paleoceanography 26, PA2224, doi:10.1029/2010PA002084.
1075
1076 Henry, L.G., McManus, J.F., Curry, W.B., Roberts, N.L., Piotrowski, A.M., Keigwin, L.D.,
1077 2016. North Atlantic ocean circulation and abrupt climate change during the last glaciation.
1078 Science 353, 470-474.
1079
1080 Hibbert, F.D., Austin, W.E.N., Leng, M.J., Gatliff, R.W., 2010. British Ice Sheet dynamics
1081 inferred from North Atlantic ice-rafted debris records spanning the last 175 000 years.
1082 Journal of Quaternary Science 25, 461-482.
1083
1084 Hunt, J.B., Hill, P.G., 2001. Tephrological implications of beam size-sample-size effects in
1085 electron microprobe analysis of glass shards. Journal of Quaternary Science 16, 105-117.
1086
1087 Jørgensen, K.A., 1980. The Thorsmork ignimbrite: An unusual comenditic pyroclastic flow
1088 in Southern Iceland. Journal of Volcanology and Geothermal Research 8, 7-22.
1089
1090 Kolling, H., Bauch, H. A., 2017. A Stratigraphical-Sedimentological Study of the Last
1091 Interglacial Period in the Central Nordic Seas on the Basis of XRF Core Scanning.
1092 Polarforschung 87, 15-22.
1093
1094 Kuehn, S.C., Froese, D.G., Shane, P.A.R., INTAV Intercomparison Participants (2011) "The
1095 INTAV intercomparison of electron-beam microanalysis of glass by tephrochronology
1096 laboratories: Results and recommendations", *Quaternary International* **246**, 19-47.
1097

Kvamme T, Mangerud J, Furnes H, Ruddiman W. 1989. Geochemistry of Pleistocene ash zones in cores from the North Atlantic. *Norsk Geologisk Tidskrift* **69**: 251-272.

Lacasse C, Sigurdsson H, Carey S, Paterne M, Guichard F. 1996. North Atlantic deep-sea sedimentation of Late Quaternary tephra from the Iceland hotspot. *Marine Geology* **129**: 207-235.

Lackschewitz, K.S., Wallrabe-Adams, H.-J., 1997. Composition and origin of volcanic ash zones in Late Quaternary sediments from the Rekjanes Ridge: evidence for ash fallout and ice-rafting. Marine Geology 136, 209-224.

Lane, C.S., Brauer, A., Blockley, S.P.E., Dulski, P., 2013. Volcanic ash reveals time-transgressive abrupt climate change during the Younger Dryas. Geology 41, 1251-1254.

Le Maitre, R.W., Bateman, P., Dudek, A., Keller, J., Lameyre, Le Bas, M.J., Sabine, P.A., Schmid, R., Sorensen, H., Streckeisen, A., Woolley, A.R., Zanettin, B., 1989. A Classification of Igneous Rocks and Glossary of Terms. Blackwell, Oxford.

Lowe, D.J., 2011. Tephrochronology and its application: A review. Quaternary Geochronology 6, 107-153.

Lowe, D.J., Shane, P.A.R., Alloway, B.V., Newnham, R.M., 2008. Fingerprints and age models for widespread New Zealand tephra marker beds erupted since 30,000 years ago: a framework for NZ-INTIMATE. Quaternary Science Reviews 27, 95-126.

Lowe, J.J., Barton, N., Blockley, S., Bronk Ramsey, C., Cullen, V.L., Davies, W., Gamble, C., Grant, K., Hardiman, M., Housley, R., Lane, C.S., Lee, S., Lewis, M., MacLeod, A., Menzies, M., Müller, W., Pollard, M., Price, C., Roberts, A.P., Rohling, E.J., Satow, C., Smith, V.C., Stringer, C.B., Tomlinson, E.L., White, D., Albert, P., Arienzo, I., Barker, G., Borić, D., Carandente, A., Civetta, L., Ferrier, C., Guadelli, J.-L., Karkanas, P., Koumouzelis, M., Müller, U.C., Orsi, G., Pross, J., Rosi, M., Shalamanov-Korobar, L., Sirakov, N., Tzedakis, P.C., 2012. Volcanic ash layers illuminate the resilience of Neanderthals and early modern humans to natural hazards. Proceedings of the National Academy of Sciences 109, 13532-13537.

Lowe, J.J., Bronk Ramsey, C., Housley, R.A., Lane, C.S., Tomlinson, E.L., RESET Team, RESET Associates, 2015. The RESET project: constructing a European tephra lattice for refined synchronisation of environmental and archaeological events during the last c. 100 ka. Quaternary Science Reviews 118, 1-17.
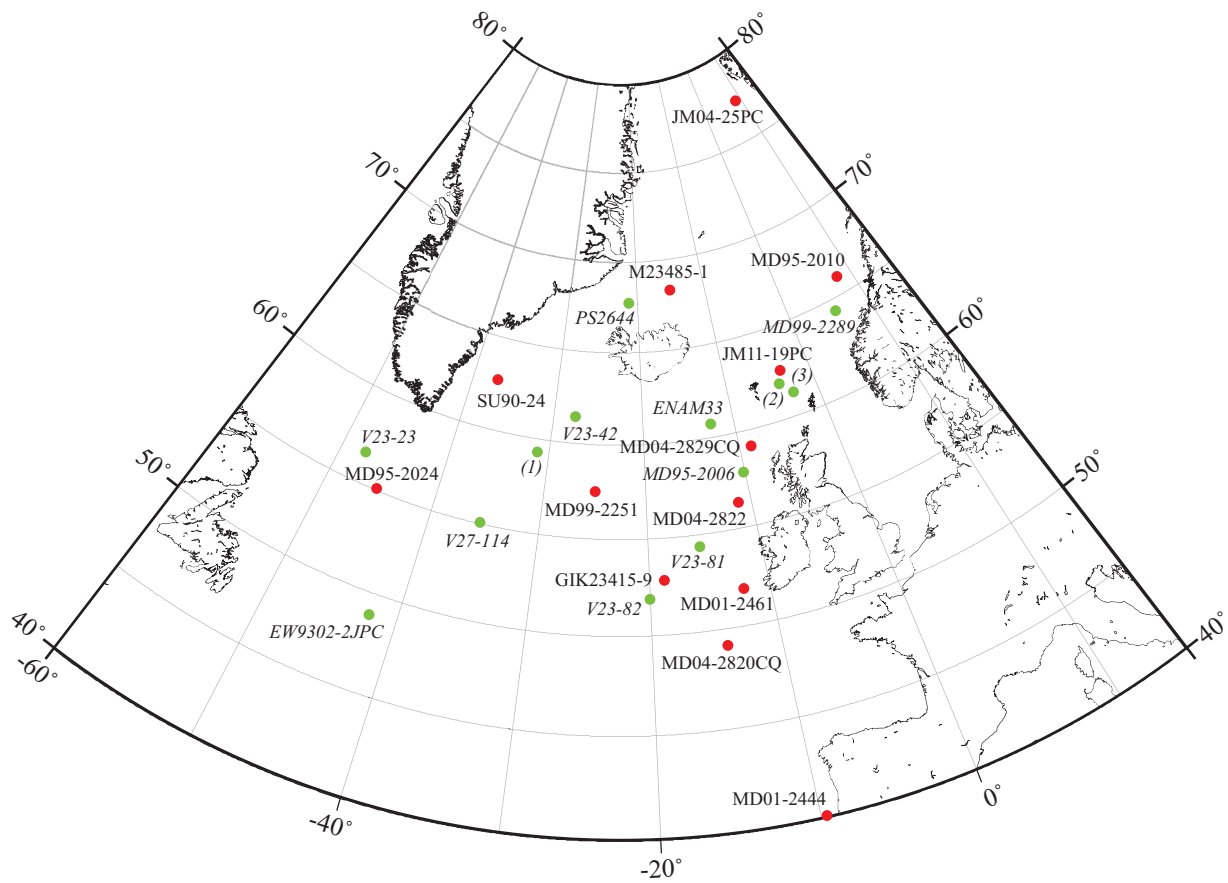
Lowe, J.J., Rasmussen, S.O., Björck, S., Hoek, W.Z., Steffensen, J.P., Walker, M.J.C., Yu, Z.C., the INTIMATE group, 2008. Synchronisation of palaeoenvironmental events in the North Atlantic region during the Last Termination: a revised protocol recommended by the INTIMATE group. Quaternary Science Reviews 27, 6-17.
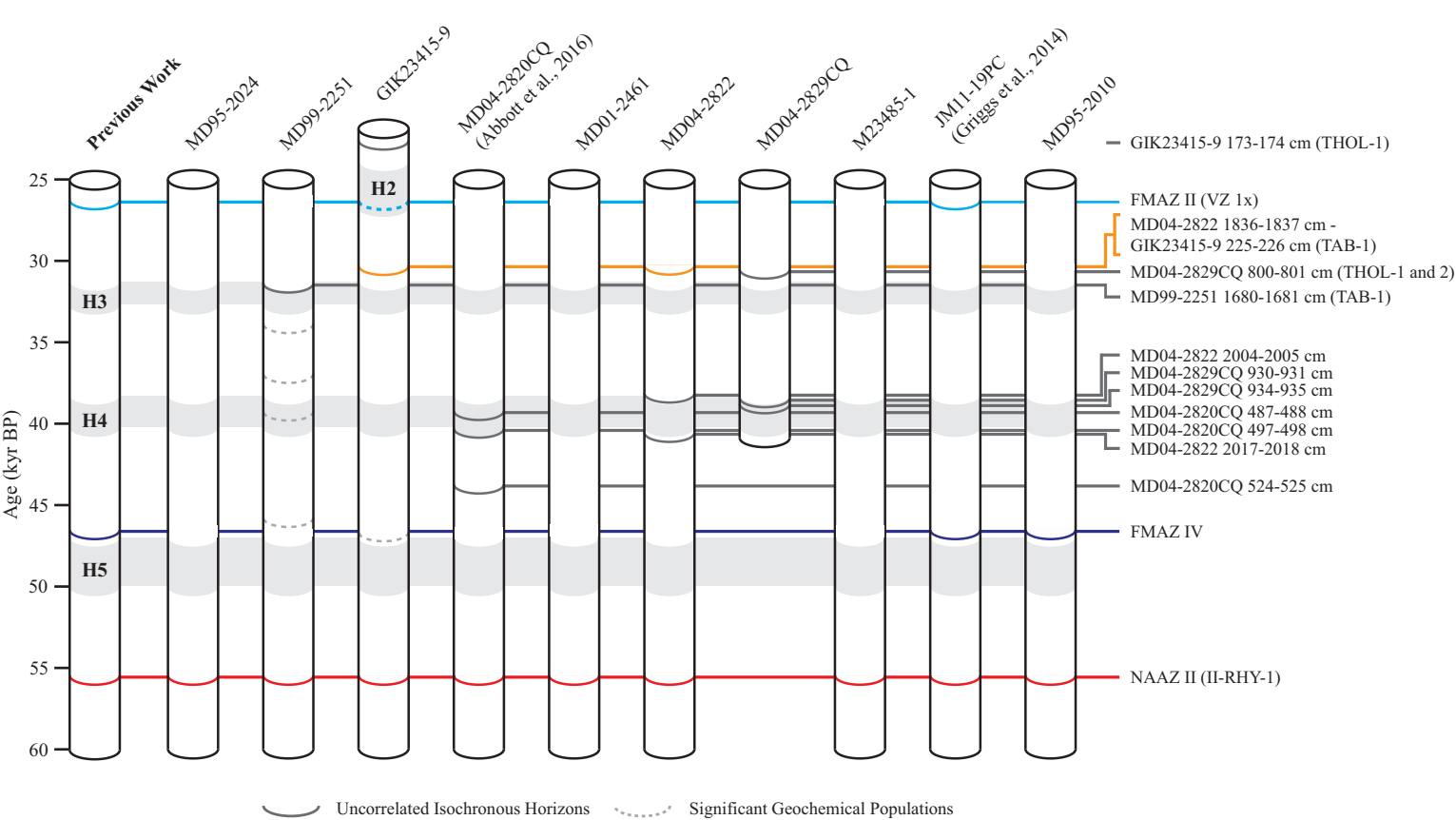
Lu, H.-Y., Wu, N.-Q., Liu, K.-B., Jiang, H., Liu, T.-S., 2007. Phytoliths as quantitative indicators for the reconstruction of past environmental conditions in China II: palaeoenvironmental reconstruction in the Loess Plateau. Quaternary Science Reviews 26, 759-772.

1148 MacDonald, G.A., Katsura, T. 1964. Chemical composition of Hawaiian lavas. Journal of
1149 Petrology 5, 83-133.

1151 Martrat, B., Grimalt, J.O., Shackleton, N.J., de Abreu, L., Hutterli, M.A. and Stocker, T.F.,
1152 2007. Four climate cycles of recurring deep and surface water destabilizations on the Iberian
1153 Margin. Science 317, 502-507.

1155 Matthews, I.P., Trincardi, F., Lowe, J.J., Bourne, A.J., Macleod, A., Abbott, P.M., Andersen,
1156 N., Asioli, A., Blockley, S.P.E., Lane, C.S., Oh, Y.A., Satow, C.S., Staff, R.A., Wulf, S.,
1157 2015. Developing a robust tephrochronological framework for Late Quaternary marine
1158 records in the Southern Adriatic Sea: new data from core station SA03-11. Quaternary
1159 Science Reviews 118, 84-104.

1161 Mortensen, A.K., Bigler, M., Grönvold, K., Steffensen, J.P., Johnsen, S.J., 2005. Volcanic
1162 ash layers from the Last Glacial Termination in the NGRIP ice core. Journal of Quaternary
1163 Science 20, 209-219.

1165 North Greenland Ice Core Project Members, 2004. High-resolution record of Northern
1166 Hemisphere climate extending into the last interglacial period. Nature 431, 147-151.

1168 Rasmussen, T.L., Wastegård, S., Kuijpers, A., van Weering, T.C.E., Heinemeier, J.,
1169 Thomsen, E., 2003. Stratigraphy and distribution of tephra layers in marine sediment cores
1170 from the Faeroe Islands, North Atlantic. Marine Geology 199, 263-277.

1172 Ruddiman W., Glover R., 1972. Vertical mixing of ice-rafted volcanic ash in North Atlantic
1173 sediments. Geological Society Bulletin 83, 2817-2836.

1175 Sanchez Goñi, M.F., Harrison, S.P., 2010. Millennial-scale climate variability and vegetation
1176 changes during the Last Glacial: concepts and terminology. Quaternary Science Reviews 29,
1177 2823-2827.

1179 Seierstad, I.K., Abbott, P.M., Bigler, M., Blunier, T., Bourne, A.J., Brook, E., Buchardt, S.L.,
1180 Buizert, C., Clausen, H.B., Cook, E., Dahl-Jensen, D., Davies, S.M., Guillevic, M., Johnsen,
1181 S.J., Pedersen, D.S., Popp, T.J., Rasmussen, S.O., Severinghaus, J.P., Svensson, A., Vinther,
1182 B.M. (2014). Consistently dated records from the Greenland GRIP, GISP2, and NGRIP ice
1183 cores for the past 104 ka reveal millennial-scale $\delta^{18}O$ gradients with possible Heinrich event
1184 imprint. Quaternary Science Reviews 106, 29-46.

1186 Timms, R.G.O., Matthews, I.P., Palmer, A.P., Candy, I., Abel, L. (2017) A high-resolution
1187 tephrostratigraphy from Quoyloo Meadow, Orkney, Scotland: Implications for the
1188 tephrostratigraphy of NW Europe during the Last Glacial-Interglacial Transition. Quaternary
1189 Geochronology 40, 67-81.

1191 Tryon, C.A., Logan, M.A.V., Mouralis, D., Kuehn, S., Slimak, L., Balkan-Atl1, N., 2009.
1192 Building a tephrostratigraphic framework for the Paleolithic of central Anatolia, Turkey.
1193 Journal of Archaeological Science 36, 637-652.

1195 Voelker, A.H.L., Haflidason, H., 2015. Refining the Icelandic tephrachronology of the last
1196 glacial period – The deep-sea core PS2644 record from the southern Greenland Sea. Global
1197 and Planetary Change 131, 35-62.

1198

1199   Vogelsang, E., Sarnthein, M., Pflaumann, U., 2004. Distribution of planktic foraminifera in
1200   sediment core GIK23415-9. DOI:10.1594/PANGAEA.186156.
1201

1202   Wastegård, S., Rasmussen, T.L., 2014. Faroe Marine Ash Zone IV: a new MIS 3 ash zone on
1203   the Faroe Islands margin. In Austin, W.E.N., Abbott, P.M., Davies, S.M., Pearce, N.J.G.,
1204   Wastegård, S., (eds) Marine Tephrochronology, Geological Society of London Special
1205   Publication 398, 81-93.
1206

1207   Wastegård S., Rasmussen T.L., Kuijpers A., Nielsen T., van Weering, T.C.E., 2006.
1208   Composition and origin of ash zones from Marine Isotope Stages 3 and 2 in the North
1209   Atlantic. Quaternary Science Reviews 25, 2409-2419.
1210

1211   Weinelt, M. (2004) Ice rafted debris of sediment core GIK23415-9.
1212   DOI:10.1594/PANGAEA.143869.
1213

1214   Zanchetta, G., Sulpizio, R., Roberts, N., Cioni, R., Eastwood, W.J., Siani, G., Caron, B.,
1215   Paterne, M., Santacroce, R., 2011. Tephrostratigraphy, chronology and climatic events of the
1216   Mediterranean basin during the Holocene: An overview. The Holocene 21, 33-52.
1217

1218   Zielinski G.A., Mayewski P.A., Meeker L.D., Gronvöld K., Germani M.S., Whitlow S.,
1219   Twickler M.S., Taylor K., 1997. Volcanic aerosol records and tephrochronology of the
1220   Summit, Greenland, ice cores. Journal of Geophysical Research 102**,** 26,625-26,640.
1221

1222   Zumaque, J., Eynaud, F., Zaragosi, S., Marret, F., Matsuzaki, K.M., Kissel, C., Roche, D.M.,
1223   Malaize, B., Michel, E., Billy, I., Richter, T., Palis, E., 2012. An ocean-ice coupled response
1224   during the last glacial: a view from a marine isotope stage 3 record south of the Faeroe
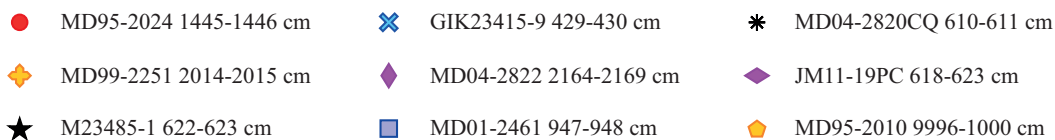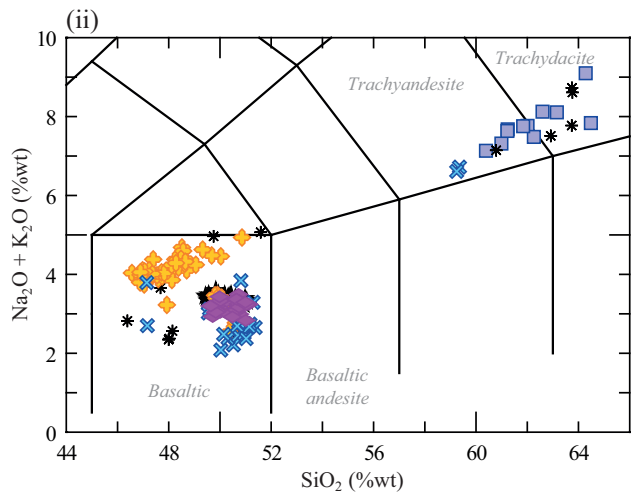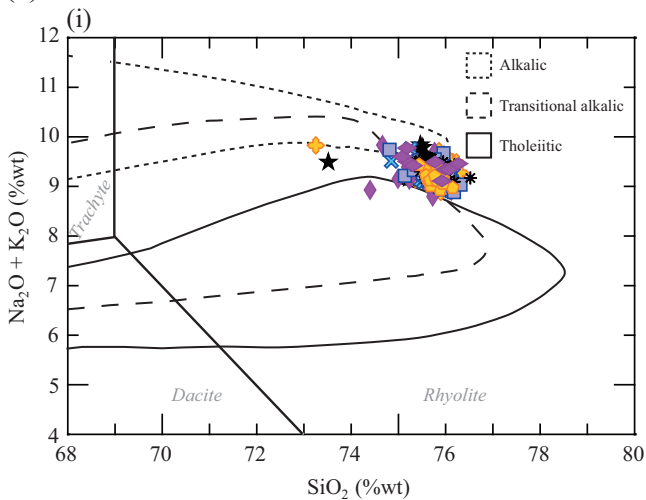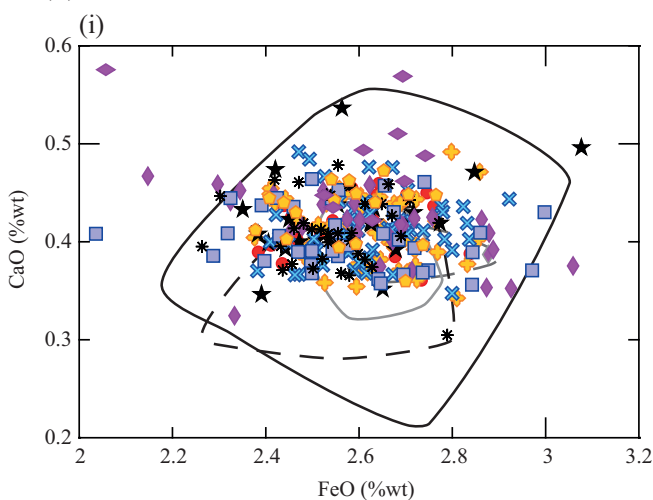1225   Shetland Gateway. Climate of the Past 8, 1997-2017.

JM04-25PC

MD95-2010

M23485-1

PS2644

MD99-2289

JM11-19PC

(3)

(2)

SU90-24

V23-23

ENAM33

V23-42

MD04-2829CQ

(1)

MD95-2006

MD95-2024

MD99-2251

MD04-2822

V27-114

V23-81

GIK23415-9

V23-82

MD01-2461

EW9302-2JPC

MD04-2820CQ

MD01-2444

Figure showing tephrostratigraphic correlations across multiple marine sediment cores (Previous Work, MD95-2024, MD99-2251, GIK23415-9, MD04-2820CQ (Abbott et al., 2016), MD01-2461, MD04-2822, MD04-2829CQ, M23485-1, JM11-19PC (Griggs et al., 2014), MD95-2010) plotted against Age (kyr BP) from 25 to 60.

Isochronous horizons labelled on the right:
- GIK23415-9 173-174 cm (THOL-1)
- FMAZ II (VZ 1x)
- MD04-2822 1836-1837 cm - GIK23415-9 225-226 cm (TAB-1)
- MD04-2829CQ 800-801 cm (THOL-1 and 2)
- MD99-2251 1680-1681 cm (TAB-1)
- MD04-2822 2004-2005 cm
- MD04-2829CQ 930-931 cm
- MD04-2829CQ 934-935 cm
- MD04-2820CQ 487-488 cm
- MD04-2820CQ 497-498 cm
- MD04-2822 2017-2018 cm
- MD04-2820CQ 524-525 cm
- FMAZ IV
- NAAZ II (II-RHY-1)

Heinrich events labelled H2, H3, H4, H5.

Legend: ⌣ Uncorrelated Isochronous Horizons   ⋯ Significant Geochemical Populations

(a)

(i) — plot of Na₂O + K₂O (%wt) vs SiO₂ (%wt) with fields labelled *Trachyte*, *Dacite*, *Rhyolite*; legend boxes: Alkalic, Transitional alkalic, Tholeiitic.

(ii) — plot of Na₂O + K₂O (%wt) vs SiO₂ (%wt) with fields labelled *Trachyandesite*, *Trachydacite*, *Basaltic*, *Basaltic andesite*.

Legend:
- ● MD95-2024 1445-1446 cm
- ✕ GIK23415-9 429-430 cm
- ✱ MD04-2820CQ 610-611 cm
- ✦ MD99-2251 2014-2015 cm
- ◆ MD04-2822 2164-2169 cm
- ◆ JM11-19PC 618-623 cm
- ★ M23485-1 622-623 cm
- ▩ MD01-2461 947-948 cm
- ⬠ MD95-2010 9996-1000 cm

(b)

(i) — plot of CaO (%wt) vs FeO (%wt).

(ii) — plot of Na₂O (%wt) vs SiO₂ (%wt).

(c)

(i) — plot of TiO₂ (%wt) vs FeO/MgO.

(ii) — plot of TiO₂ (%wt) vs CaO (%wt).

II-RHY-1:
- ⬭ Kvamme et al. (1989)
- ⬭ Austin et al. (2004)
- ⬭ (dashed) Wastegård et al. (2006)
- ⬭ (dashed) Brendryen et al. (2011)

Kvamme et al. (1989):
- II-THOL-1
- II-THOL-3
- II-THOL-2
- II-TAB-1

Rhyolitic Shards (25-80 μm)

Basaltic Shards (25-80 μm)

(i)

(ii)

(b)

Marine Deposits

Rhyolitic material

Basaltic material

No NAAZ II Tephra

1000000
10000
100

shards per 0.5g dws (25-80 μm)

(c)

M23485-1

JM11-19PC

MD99-2251

MD01-2461

GIK23415-9

MD04-2820CQ

II-THOL-1

II-THOL-2

II-TAB-1

II-INT-1

Uncorr.

(a) *MD95-2010 910-920 cm*

Brown Shards per 0.5 gdw sediment

25-80 μm   80-125 μm   >125 μm

(b)

(i)

(ii)

FMAZ IV (JM11-19PC 542-543 cm)

MD95-2010 915-916 cm

(a) *MD04-2822 (Rockall Trough)*
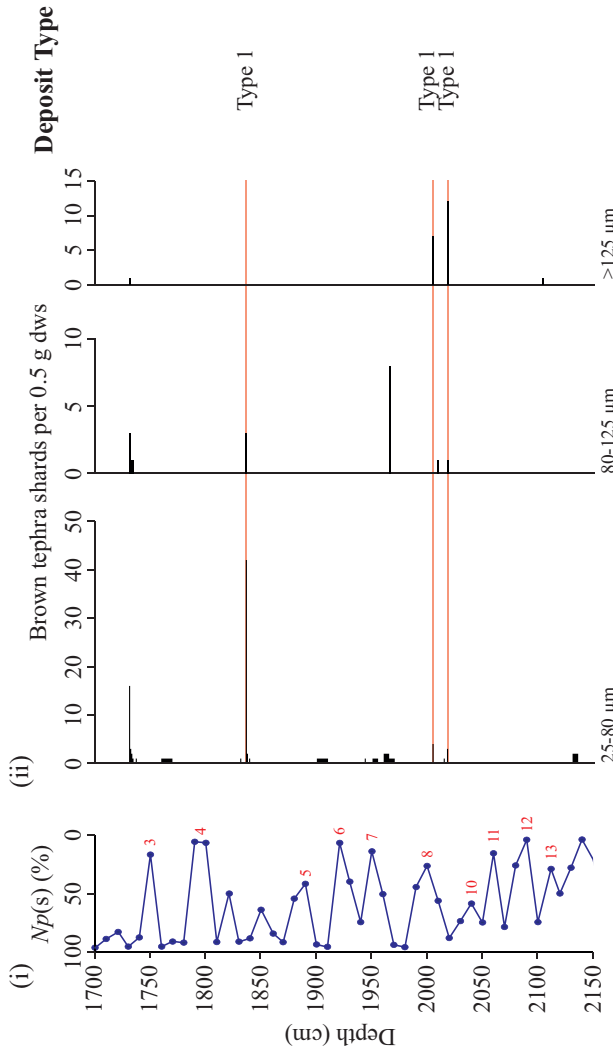
(b) *MD04-2829CQ (Rosemary Bank)*

Deposit Type

Type 1

Type 1
Type 1

Brown tephra shards per 0.5 g dws

25-80 μm   80-125 μm   >125 μm

(i) $Np(s)$ (%)

Depth (cm)

(c) *MD04-2822 and MD04-2829CQ Characterisations*

(i)

Na₂O + K₂O (%wt)

Alkaline series

Basaltic

Tholeiitic series

SiO₂ (%wt)

(ii)

FeO/TiO₂

SiO₂ (%wt)

(iii)

TiO₂ (%wt)

Al₂O₃ (%wt)

MD04-2822:

● 800-801 cm - THOL-1   ○ 1836-1837 cm   ✖ 2004-2005 cm   ✚ 2017-2018 cm   ⬡ 934-935 cm

▽ 800-801 cm - THOL-2   ◆ 930-931 cm   ◀ Veidivötn-Bárdarbunga

MD04-2829CQ:

▷ 800-801 cm - THOL-2

○ Grímsvötn   ⌇ Hekla/Vatnafjöll   ○ Katla   ⬡ Kverkfjöll   ⬡ Veidivötn-Bárdarbunga   ⬡ Vestmannaeyjar

(a) *MD99-2251 Tephrostratigraphy (Gardar Drift)*

(i) *Np*(s) (%)

(ii)

(iii)

Brown shards per 0.5 g dws

Deposit Type

Ash Free IRD per g
(100s)

25-80 μm

80-125 μm

>125 μm

Type 2B
Type 2A
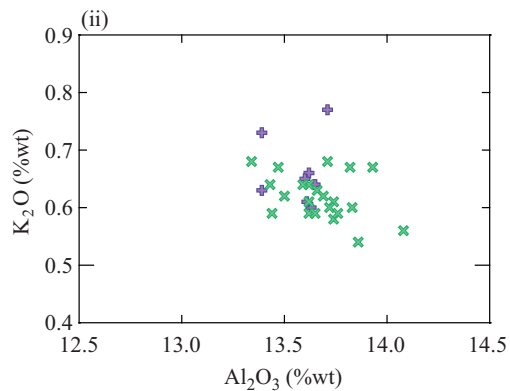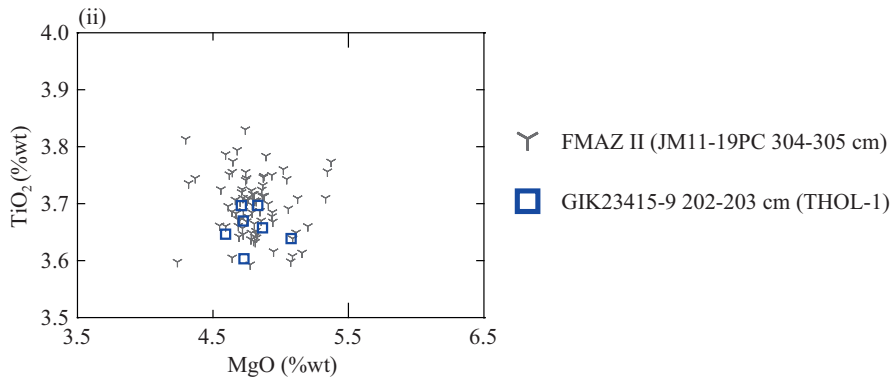Type 2B
Type 2B
Type 2B
Type 2B
Type 2B

H3
H4
H5

(b) *MD99-2251 Isochronous Horizon and Significant Geochemical Populations*

(i)

Trachybasalt
Alkaline series
Basaltic
Tholeiitic series
Basaltic andesite

(ii)

(iii)

Legend:
- ■ MD99-2251 1680-1681 cm - TAB-1
- ● MD99-2251 1713-1714 cm - TAB-1
- ○ MD99-2251 1713-1714 cm - THOL-1
- ✦ MD99-2251 1772-1773 cm - TAB-1
- ✧ MD99-2251 1772-1773 cm - TAB-2
- ✕ MD99-2251 1812-1813 cm - THOL-1
- ✕ MD99-2251 1812-1813 cm - THOL-2
- ▲ MD99-2251 1812-1813 cm - THOL-3
- △ MD99-2251 1812-1813 cm - TAB-1
- ✚ MD99-2251 1904-1905 cm - ALK-1

Grímsvötn   Hekla/Vatnafjöll   Kverkfjöll

Katla   Vestmannaeyjar   Veidivötn-Bárdarbunga

(a) *GIK23415-9 Tephrostratigraphy (Northern North Atlantic)*

(b) *GIK23415-9 Isochronous Horizons and Significant Geochemical Populations*

GIK 23415-9 173-174 cm - THOL-1
GIK 23415-9 225-226 cm - TA 2
GIK 23415-9 202-203 cm - TAB-1
GIK 23415-9 302-303 cm - THOL-1
GIK 23415-9 202-203 cm - THOL-1
GIK 23415-9 305-306 cm - THOL-1
GIK 23415-9 202-203 cm - THOL-2
GIK 23415-9 305-306 cm - THOL-2
GIK 23415-9 202-203 cm - THOL-3
GIK 23415-9 375-376 cm - THOL-1
GIK 23415-9 225-226 cm - TAB-1

Grímsvötn
Hekla/Vatnafjöll
Kverkfjöll

Katla
Vestmannaeyjar
Veidivötn-Bárdarbunga

(a)

(i)

(ii)

MD04-2822 1836-1837 cm

GIK23415-9 225-226 cm (TAB-1)

(b)

(i)

(ii)

FMAZ II (JM11-19PC 304-305 cm)

GIK23415-9 202-203 cm (THOL-1)

Tephra Horizon/Deposit (Pop.)	Climatic Event	Composition	Volcanic Source	Deposit Type	Ref(s)
Isochronous Horizons					
GIK23415-9 173-174 cm (THOL-1)	Post H2	Tholeiitic bas	Kverkfjöll	1	1
FMAZ II	Post DO-3	Transitional alkali bas	Hekla/Vatnafjöll	2A	2, 3, 4, 5
MD04-2822 1836-1837 cm	Pre DO-4	Transitional alkali bas	Katla or Hekla/Vatnafjöll	1	1
GIK23415-9 225-226 cm (TAB-1)	H3	Transitional alkali bas	Katla or Hekla/Vat.	1	1
MD04-2829CQ 800-801 cm (THOL-1)	Pre DO-4	Tholeiitic bas	Grímsvötn	1	1
MD04-2829CQ 800-801 cm (THOL-2)	Pre DO-4	Tholeiitic bas	Kverkfjöll	1	1
MD99-2251 1680-1681 cm (TAB-1)	H3	Transitional alkali bas	Katla	2A	1
MD04-2822 2004-2005 cm	DO-8	Transitional alkali bas	Katla	1	1
MD04-2829CQ 930-931 cm	DO-8	Tholeiitic bas	Grímsvötn	1	1
MD04-2829CQ 934-935 cm	Pre DO-8	Tholeiitic bas	Grímsvötn	1	1
MD04-2820CQ 487-488 cm	Pre DO-8 (H4)	Tholeiitic bas	Grímsvötn	2A	6
MD04-2820CQ 497-498 cm	Pre DO-9	Transitional alkali rhy	Katla	2A	6
MD04-2822 2017-2018 cm	Pre DO-9	Tholeiitic bas	Grímsvötn	1	1
MD04-2820CQ 524-525 cm	Pre DO-11	Tholeiitic bas	Grímsvötn or Kverkfjöll	2A	6
FMAZ IV	Pre DO-12	Tholeiitic bas	Grímsvötn	2A	5, 7
NAAZ II (II-RHY-1)	End of DO-15	Transitional alkali rhy	Tindfjallajökull	3	1, 3, 8, 9, 10
Significant Geochemical Populations					
GIK23415-9 202-203 cm (TAB-1)	*Pre H2*	*Transitional alkali bas*	*Katla*	*2B*	*1*
GIK23415-9 202-203 cm (THOL-1)	*Pre H2*	*Tholeiitic bas*	*Kverkfjöll*	*2B*	*1*
GIK23415-9 202-203 cm (THOL-2)	*Pre H2*	*Tholeiitic bas*	*Grímsvötn*	*2B*	*1*
GIK23415-9 202-203 cm (THOL-3)	*Pre H2*	*Tholeiitic bas*	*Veid. -Bárd.*	*2B*	*1*
MD99-2251 1713-1714 cm (TAB-1)	*Pre H3*	*Transitional alkali bas*	*Katla*	*2B*	*1*
MD99-2251 1713-1714 cm (THOL-1)	*Pre H3*	*Tholeiitic bas*	*Grímsvötn*	*2B*	*1*
MD99-2251 1772-1773 cm (TAB-1)	*Post H4*	*Transitional alkali bas*	*Katla*	*2B*	*1*
MD99-2251 1772-1773 cm (TAB-2)	*Post H4*	*Transitional alkali bas*	*Katla (?)*	*2B*	*1*
GIK23415-9 302-306 cm (THOL-1)	*H4*	*Tholeiitic bas*	*Grímsvötn*	*4*	*1*
GIK23415-9 302-306 cm (THOL-2)	*H4*	*Tholeiitic bas*	*Grímsvötn (?)*	*4*	*1*
MD99-2251 1812-1813 cm (THOL-1)	*H4*	*Tholeiitic bas*	*Grímsvötn*	*2B*	*1*
MD99-2251 1812-1813 cm (THOL-2)	*H4*	*Tholeiitic bas*	*Veid. -Bárd.*	*2B*	*1*
MD99-2251 1812-1813 cm (THOL-3)	*H4*	*Tholeiitic bas*	*Veid. -Bárd.*	*2B*	*1*
MD99-2251 1812-1813 cm (TAB-1)	*H4*	*Transitional alkali bas*	*Katla*	*2B*	*1*
MD99-2251 1904-1905 cm (ALK-1)	*Post H5*	*Alkali bas*	*Vestmannaeyjar*	*2B*	*1*
GIK23415-9 375-376 cm (THOL-1)	*Pre H5*	*Tholeiitic bas*	*Grímsvötn*	*2B*	*1*

Table 1: Summary of isochronous horizons and significant geochemical populations forming the marine tephra framework for the North Atlantic between 25-60 ka BP. The designation of climatic events is based on pre-existing stratigraphic frameworks for the cores. The stratigraphic ordering of horizons between cores is approximate. FMAZ II, FMAZ IV and NAAZ II have been identified in multiple cores. H = Heinrich Event; DO = Dansgaard-Oeschger Event. bas = basaltic; rhy = rhyolitic. Vat. = Vatnafjöll; Veid.-Bárd. = Veidivötn-Bárdarbunga. Deposit types based on the classification scheme outlined in Abbott et al. (submitted). References are as follows: 1: this study; 2: Rasmussen et al. (2003); 3: Wastegård et al. (2006); 4: Davies et al. (2008); 5: Griggs et al. (2014); 6: Abbott et al. (2016); 7: Wastegård and Rasmussen (2014); 8: Kvamme et al. (1989); 9: Austin et al. (2004); 10: Brendryen et al. (2010).
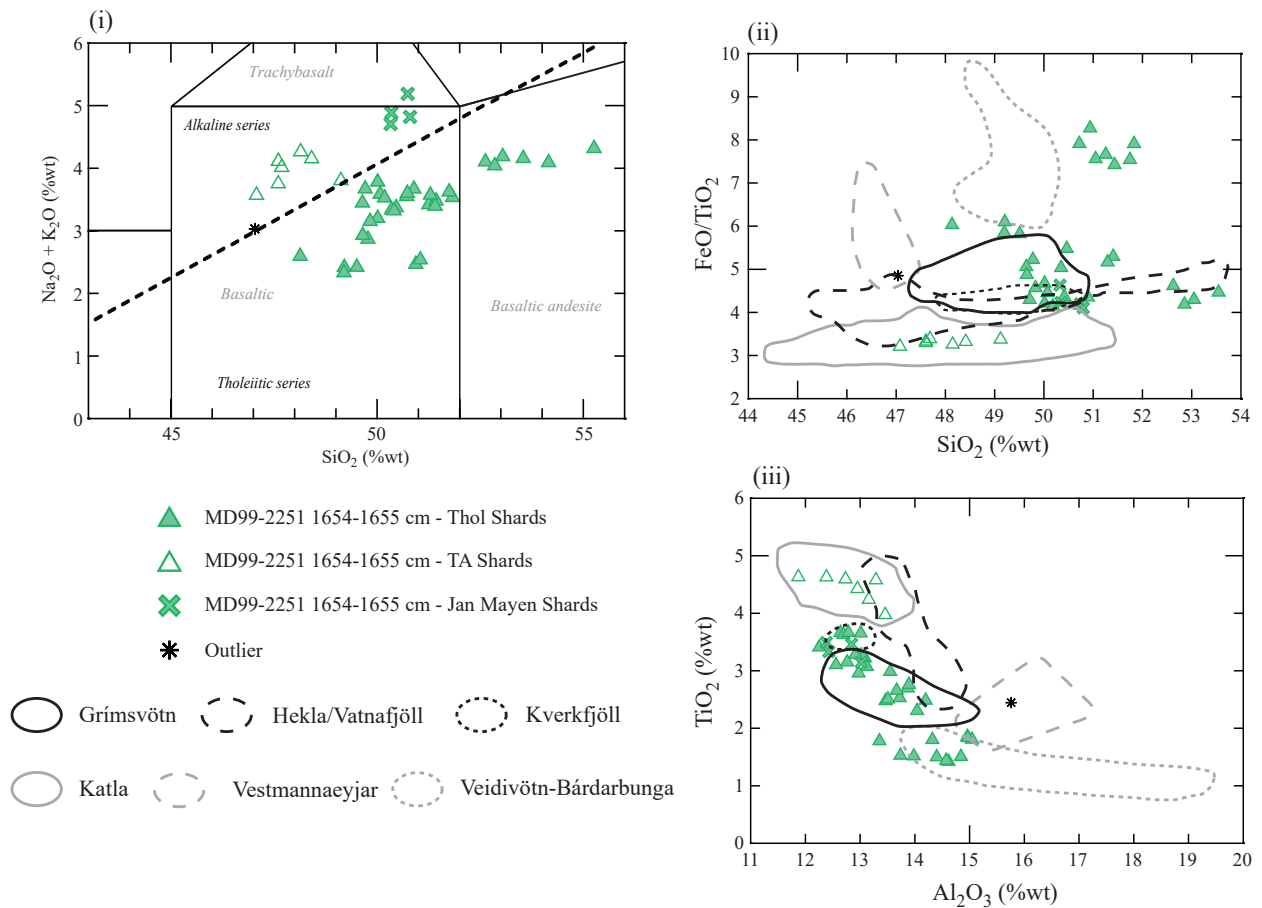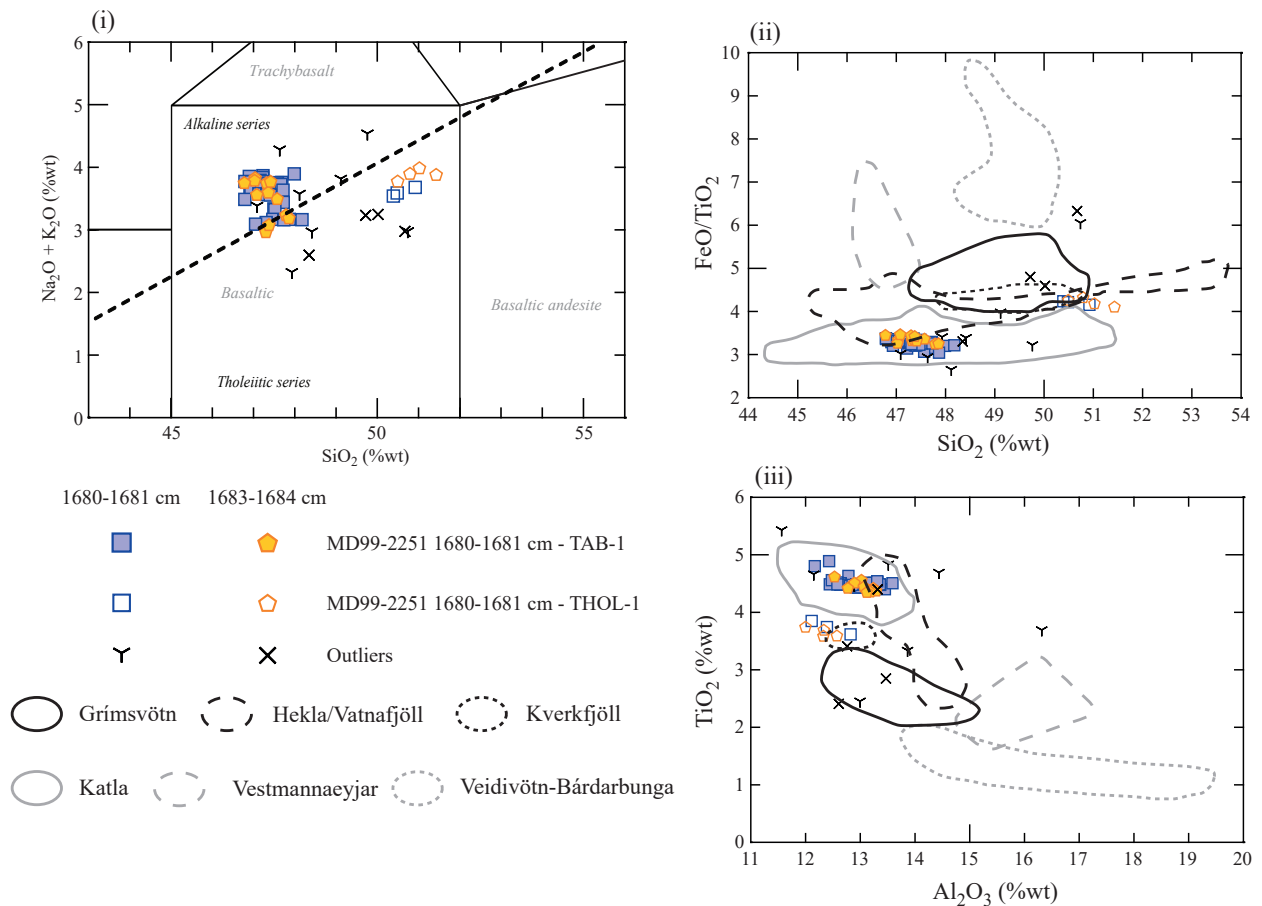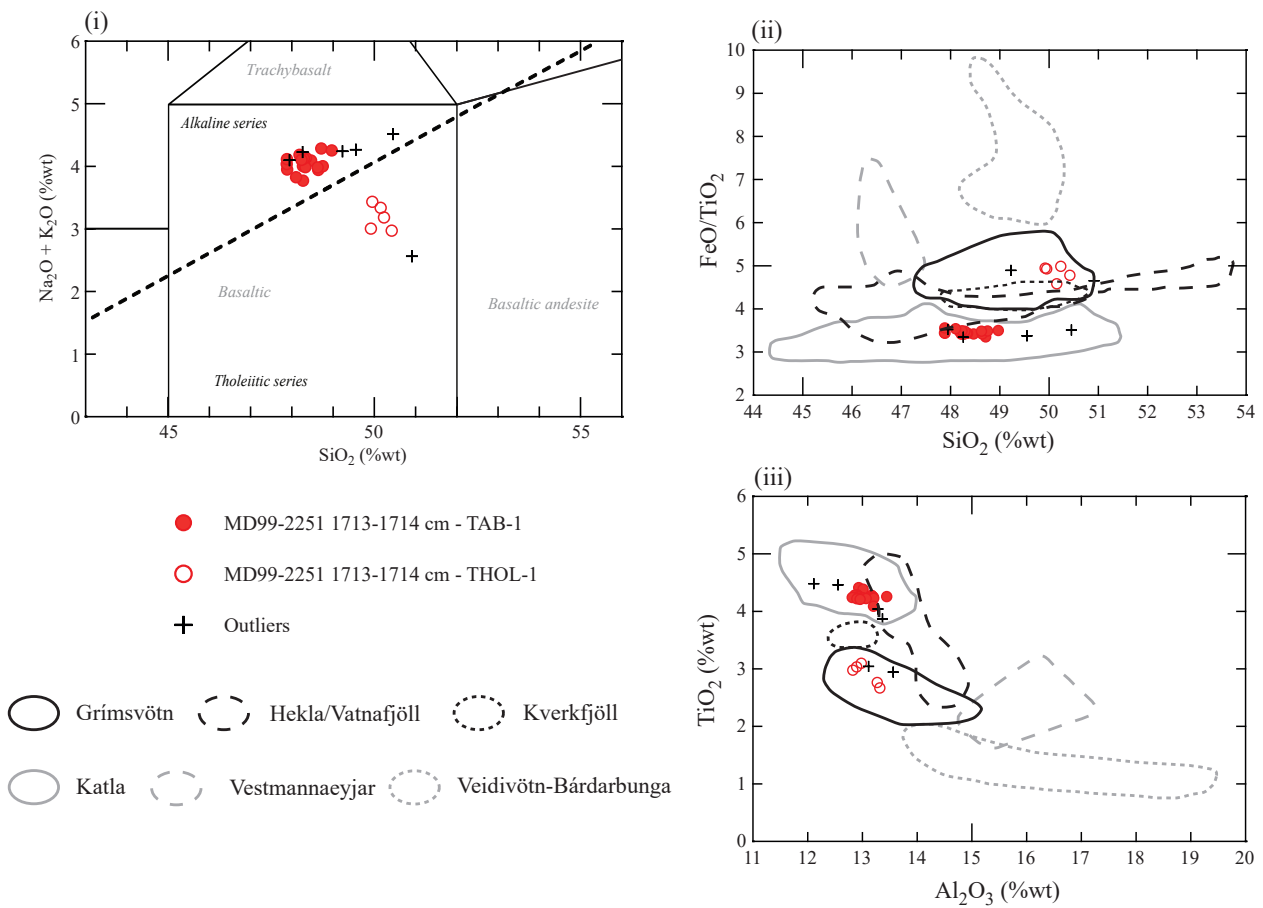
Supplementary Figures

Figure S1: Geochemical populations identified within shard analyses from the MD99-2251 1654-1655 cm deposit. (i) inset of total alkali vs. silica plot. Division line to separate alkaline and sub-alkaline material from MacDonald and Katsura (1964). Chemical classification and nomenclature after Le Maitre et al. (1989). (ii) FeO/TiO$_2$ vs. SiO$_2$ and (iii) TiO$_2$ vs. Al$_2$O$_3$ compositional variation diagrams comparing populations to characterisations of proximal Icelandic material. Geochemical fields for Icelandic source volcanoes are based on those utilised in Bourne et al. (2015) and references within.
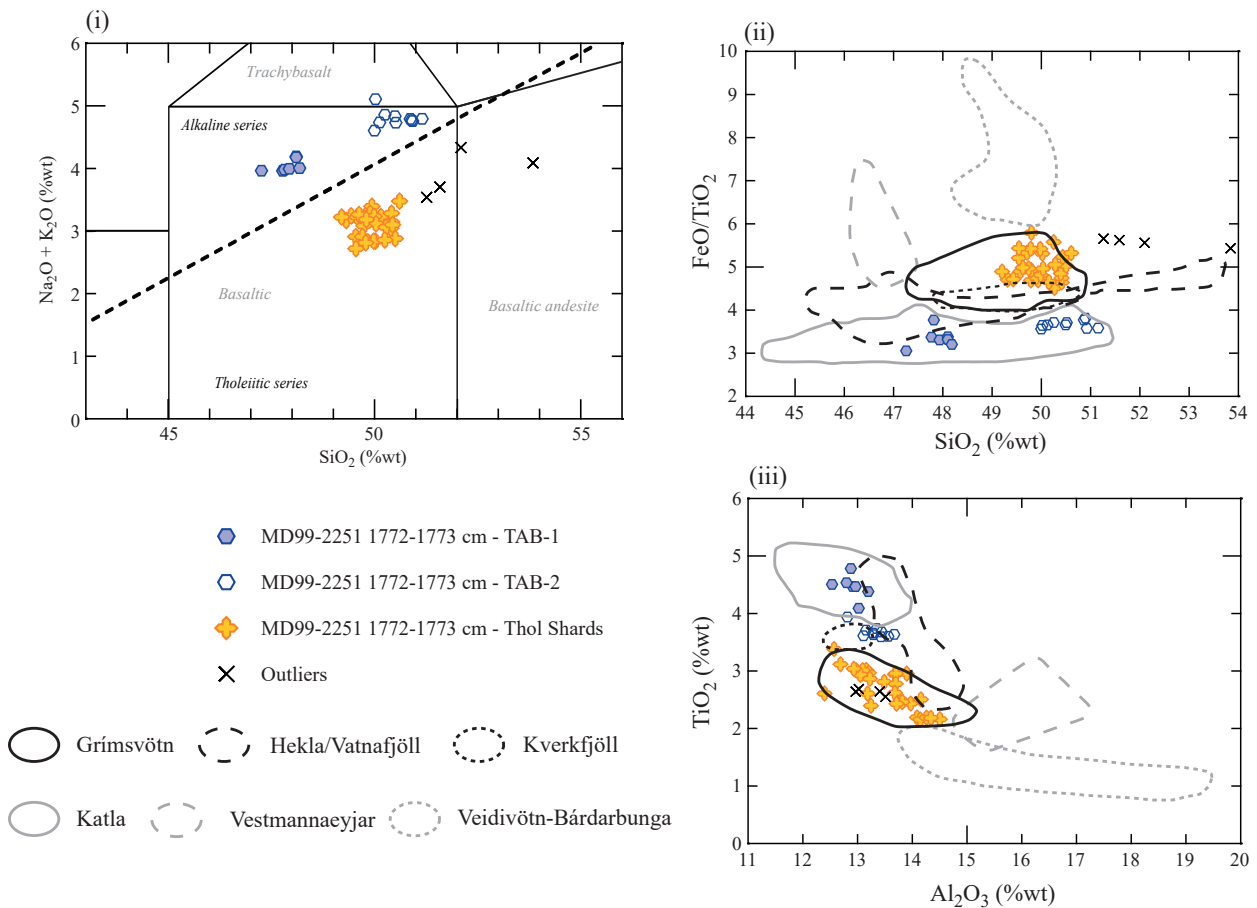

Figure S2: Geochemical populations identified within shard analyses from the MD99-2251 1680-1681 cm deposit. (i) inset of total alkali vs. silica plot. Division line to separate alkaline and sub-alkaline material from MacDonald and Katsura (1964). Chemical classification and nomenclature after Le Maitre et al. (1989). (ii) FeO/TiO$_2$ vs. SiO$_2$ and (iii) TiO$_2$ vs. Al$_2$O$_3$ compositional variation diagrams comparing populations to characterisations of proximal Icelandic material. Geochemical fields for Icelandic source volcanoes are based on those utilised in Bourne et al. (2015) and references within.
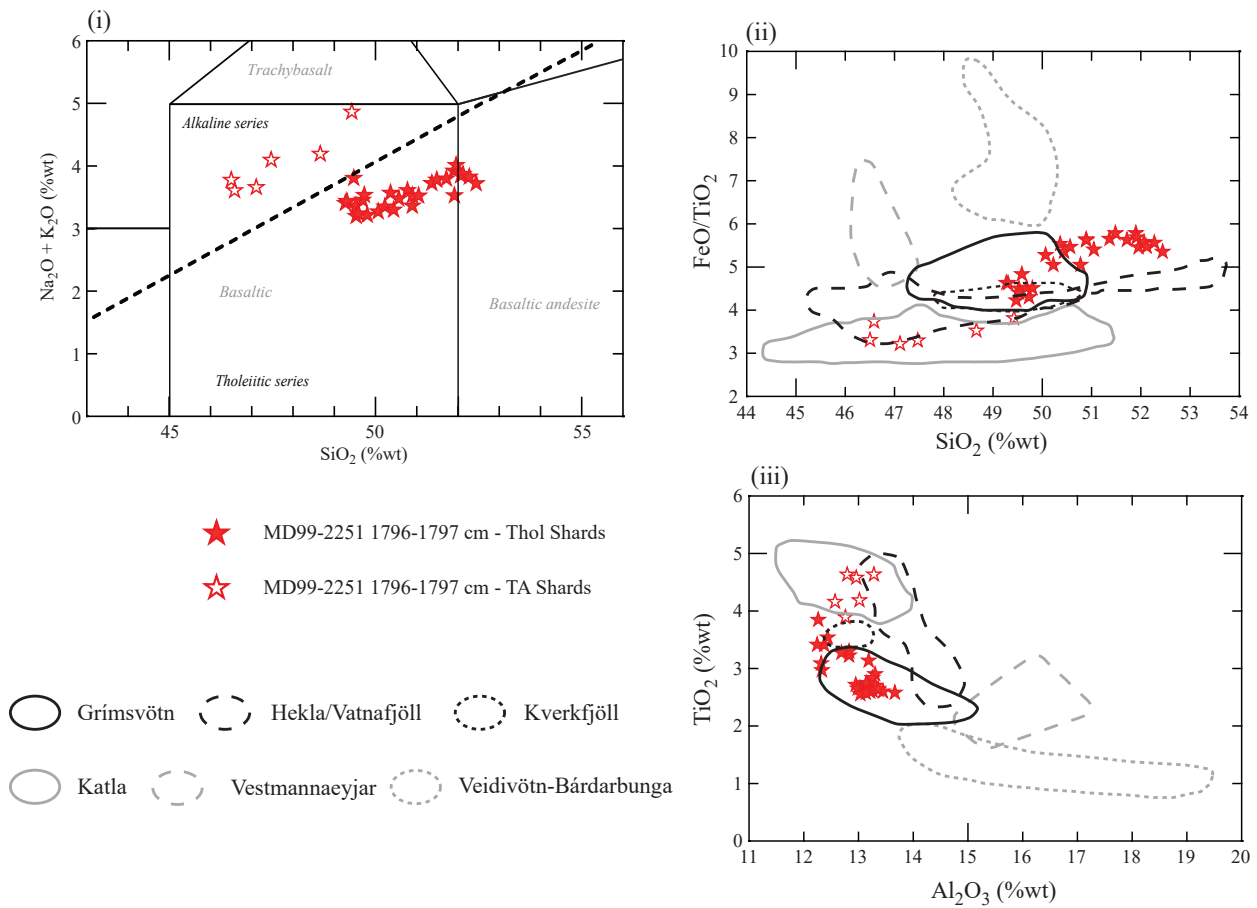
Figure S3: Geochemical populations identified within shard analyses from the MD99-2251 1713-1714 cm deposit. (i) inset of total alkali vs. silica plot. Division line to separate alkaline and sub-alkaline material from MacDonald and Katsura (1964). Chemical classification and nomenclature after Le Maitre et al. (1989). (ii) FeO/TiO$_2$ vs. SiO$_2$ and (iii) TiO$_2$ vs. Al$_2$O$_3$ compositional variation diagrams comparing populations to characterisations of proximal Icelandic material. Geochemical fields for Icelandic source volcanoes are based on those utilised in Bourne et al. (2015) and references within.
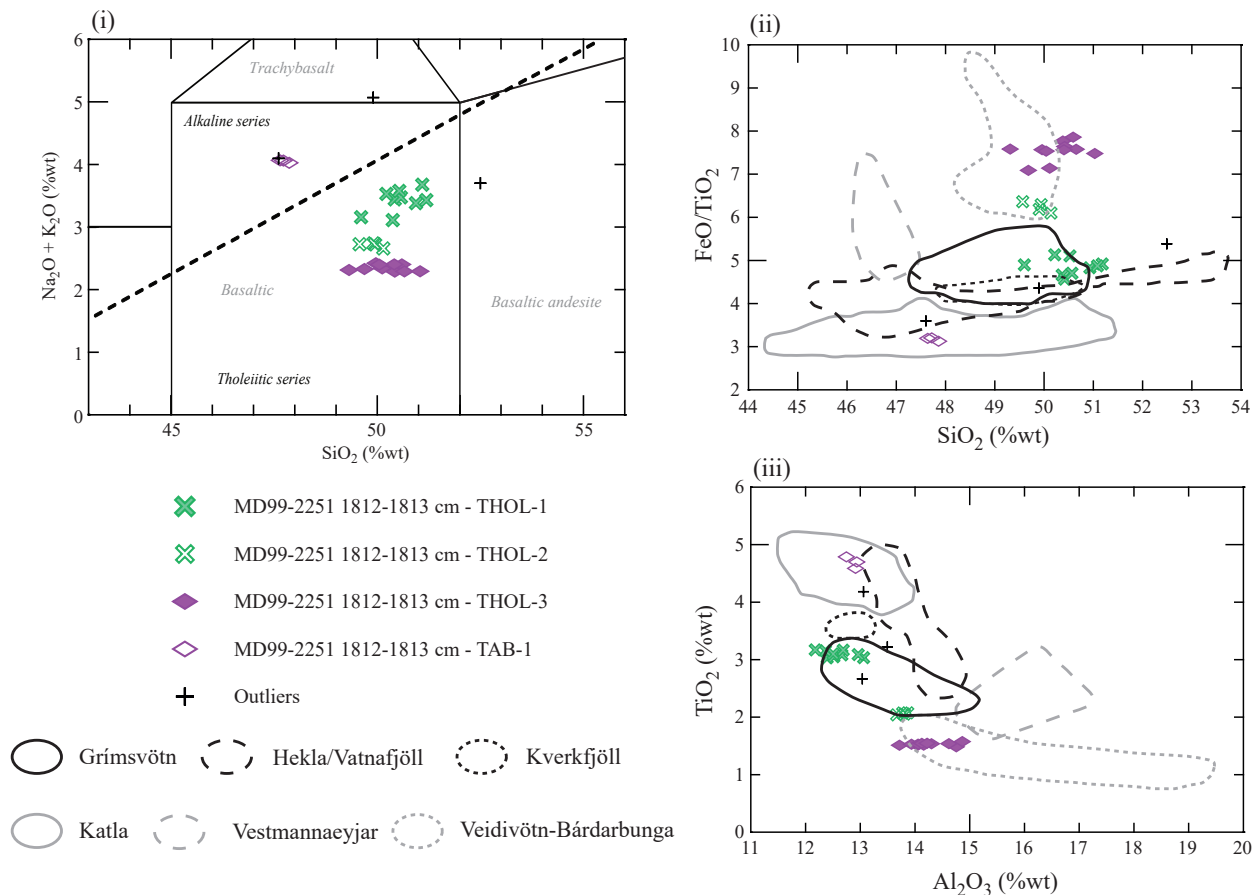

Figure S4: Geochemical populations identified within shard analyses from the MD99-2251 1772-1773 cm deposit. (i) inset of total alkali vs. silica plot. Division line to separate alkaline and sub-alkaline material from MacDonald and Katsura (1964). Chemical classification and nomenclature after Le Maitre et al. (1989). (ii) FeO/TiO$_2$ vs. SiO$_2$ and (iii) TiO$_2$ vs. Al$_2$O$_3$ compositional variation diagrams comparing populations to characterisations of proximal Icelandic material. Geochemical fields for Icelandic source volcanoes are based on those utilised in Bourne et al. (2015) and references within.
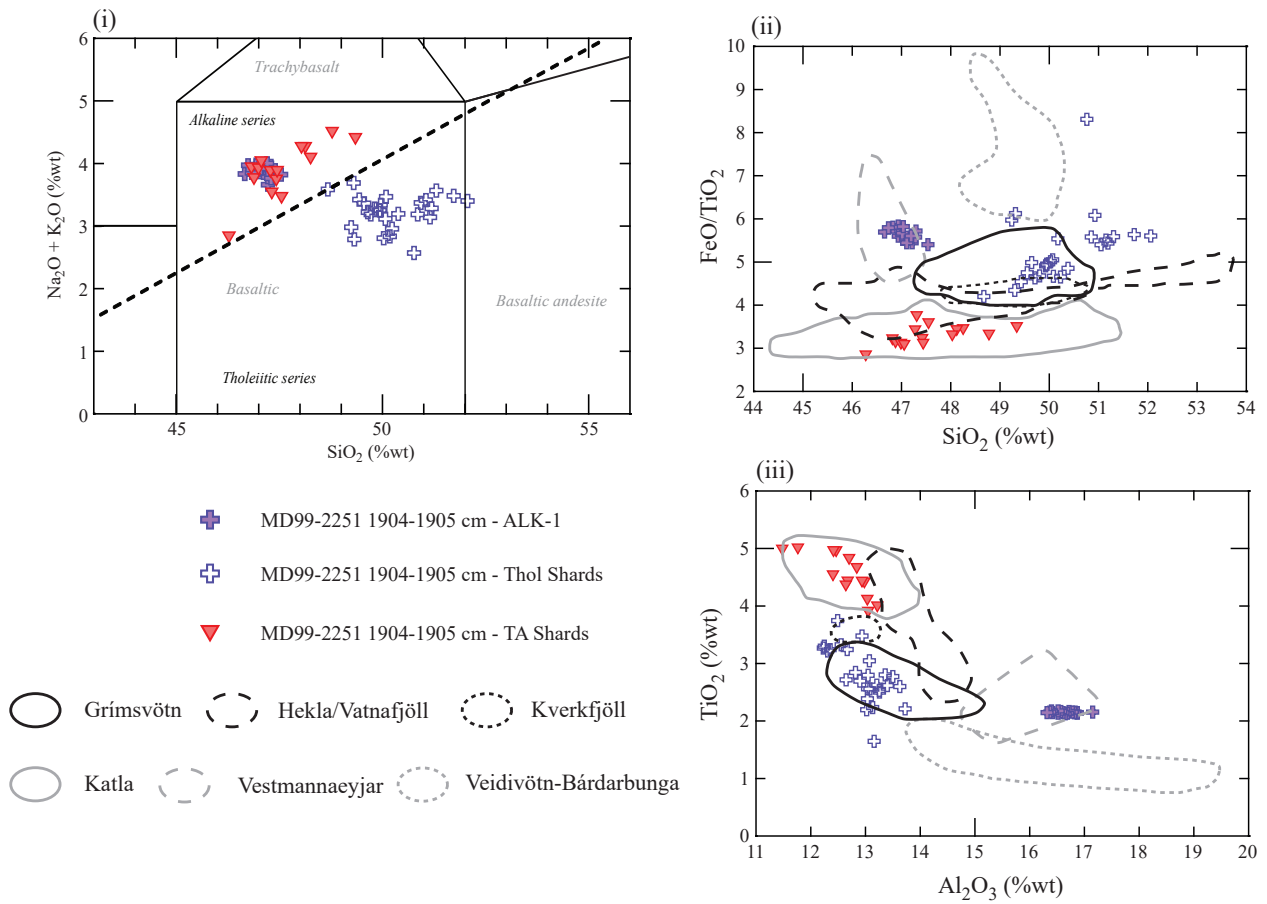
Figure S5: Geochemical populations identified within shard analyses from the MD99-2251 1796-1797 cm deposit. (i) inset of total alkali vs. silica plot. Division line to separate alkaline and sub-alkaline material from MacDonald and Katsura (1964). Chemical classification and nomenclature after Le Maitre et al. (1989). (ii) FeO/TiO$_2$ vs. SiO$_2$ and (iii) TiO$_2$ vs. Al$_2$O$_3$ compositional variation diagrams comparing populations to characterisations of proximal Icelandic material. Geochemical fields for Icelandic source volcanoes are based on those utilised in Bourne et al. (2015) and references within.

Figure S6: Geochemical populations identified within shard analyses from the MD99-2251 1812-1813 cm deposit. (i) inset of total alkali vs. silica plot. Division line to separate alkaline and sub-alkaline material from MacDonald and Katsura (1964). Chemical classification and nomenclature after Le Maitre et al. (1989). (ii) FeO/TiO$_2$ vs. SiO$_2$ and (iii) TiO$_2$ vs. Al$_2$O$_3$ compositional variation diagrams comparing populations to characterisations of proximal Icelandic material. Geochemical fields for Icelandic source volcanoes are based on those utilised in Bourne et al. (2015) and references within.
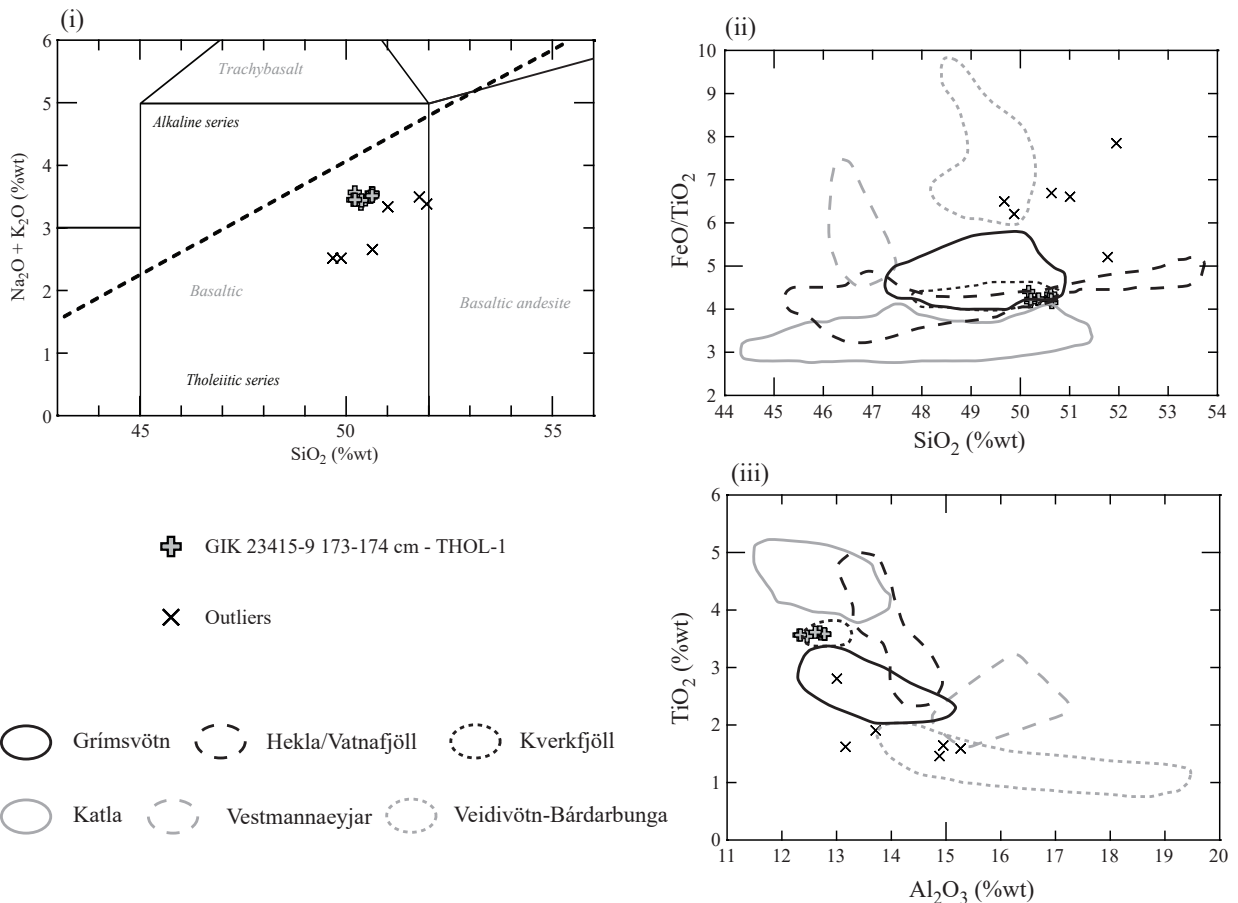
Figure S7: Geochemical populations identified within shard analyses from the MD99-2251 1904-1905 cm deposit. (i) inset of total alkali vs. silica plot. Division line to separate alkaline and sub-alkaline material from MacDonald and Katsura (1964). Chemical classification and nomenclature after Le Maitre et al. (1989). (ii) FeO/TiO_2 vs. SiO_2 and (iii) TiO_2 vs. Al_2O_3 compositional variation diagrams comparing populations to characterisations of proximal Icelandic material. Geochemical fields for Icelandic source volcanoes are based on those utilised in Bourne et al. (2015) and references within.
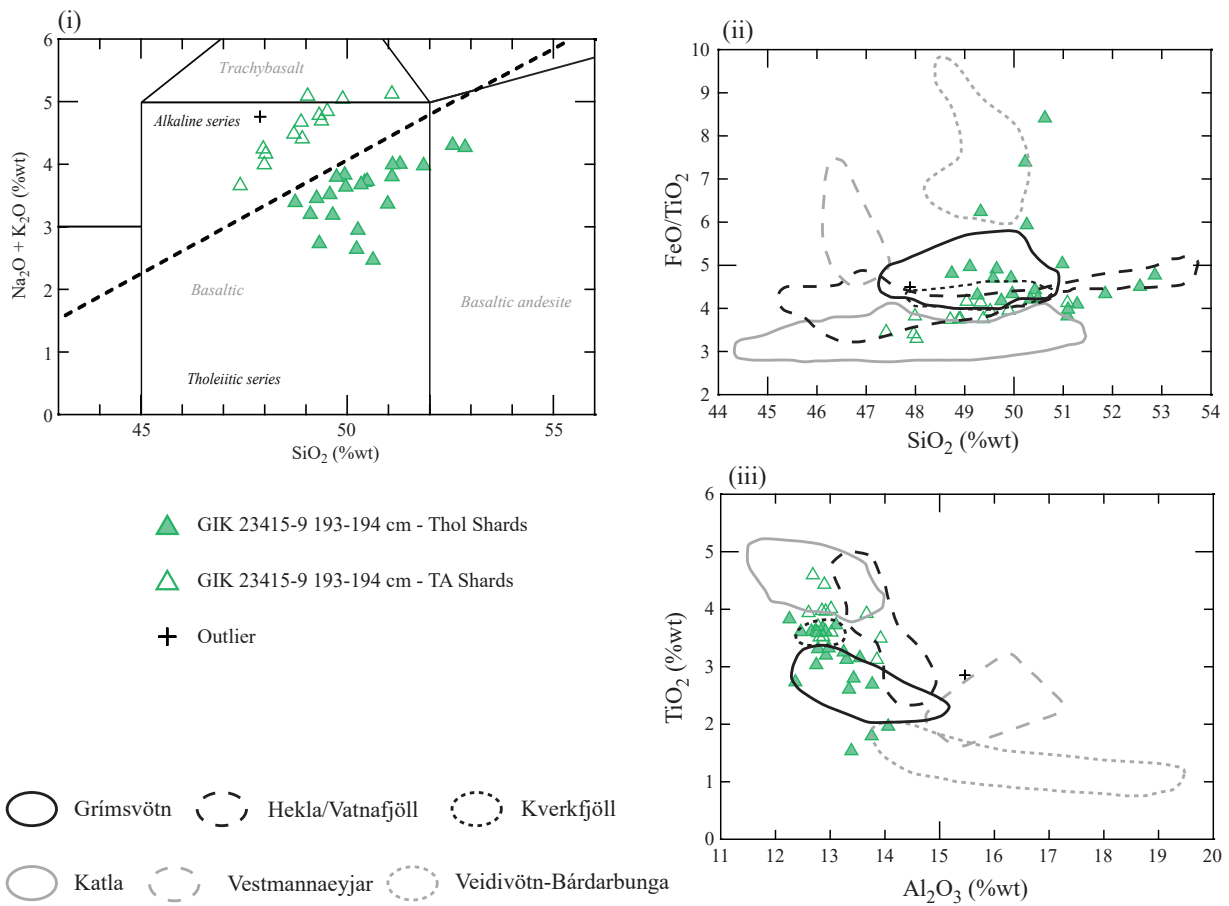

Figure S8: Geochemical populations identified within shard analyses from the GIK23415-9 173-174 cm deposit. (i) inset of total alkali vs. silica plot. Division line to separate alkaline and sub-alkaline material from MacDonald and Katsura (1964). Chemical classification and nomenclature after Le Maitre et al. (1989). (ii) FeO/TiO_2 vs. SiO_2 and (iii) TiO_2 vs. Al_2O_3 compositional variation diagrams comparing populations to characterisations of proximal Icelandic material. Geochemical fields for Icelandic source volcanoes are based on those utilised in Bourne et al. (2015) and references within.
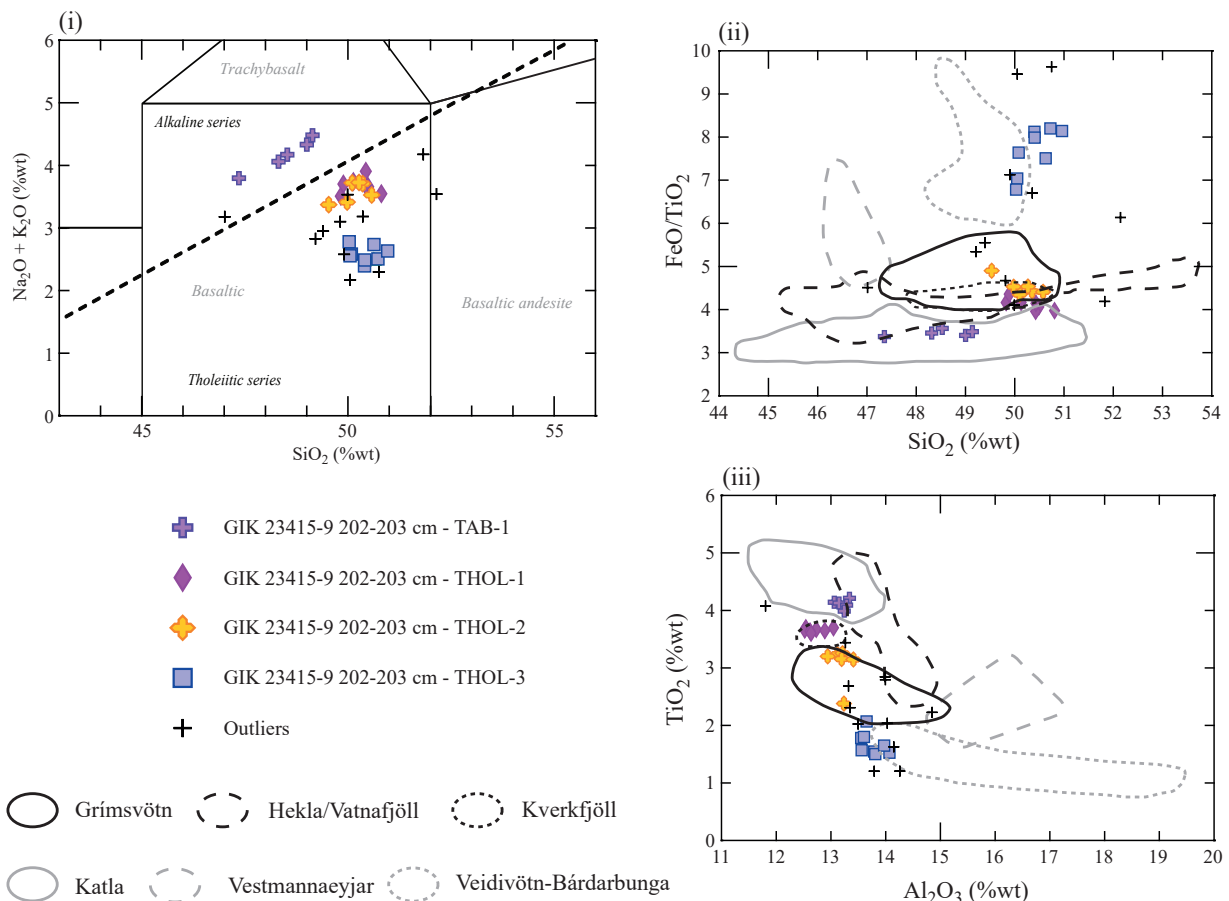
Figure S9: Geochemical populations identified within shard analyses from the GIK23415-9 193-194 cm deposit. (i) inset of total alkali vs. silica plot. Division line to separate alkaline and sub-alkaline material from MacDonald and Katsura (1964). Chemical classification and nomenclature after Le Maitre et al. (1989). (ii) FeO/TiO_2 vs. SiO_2 and (iii) TiO_2 vs. Al_2O_3 compositional variation diagrams comparing populations to characterisations of proximal Icelandic material. Geochemical fields for Icelandic source volcanoes are based on those utilised in Bourne et al. (2015) and references within.
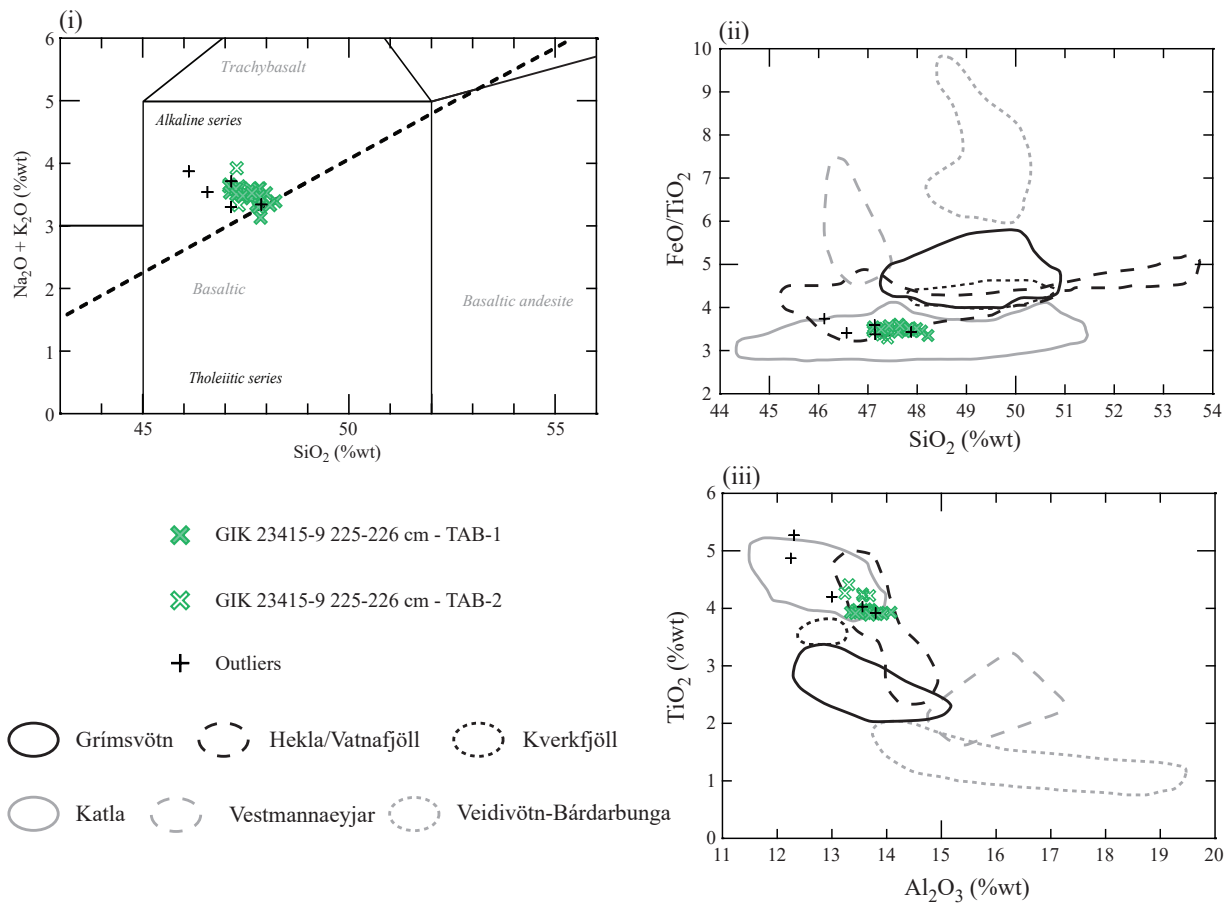

Figure S10: Geochemical populations identified within shard analyses from the GIK23415-9 202-203 cm deposit. (i) inset of total alkali vs. silica plot. Division line to separate alkaline and sub-alkaline material from MacDonald and Katsura (1964). Chemical classification and nomenclature after Le Maitre et al. (1989). (ii) FeO/TiO_2 vs. SiO_2 and (iii) TiO_2 vs. Al_2O_3 compositional variation diagrams comparing populations to characterisations of proximal Icelandic material. Geochemical fields for Icelandic source volcanoes are based on those utilised in Bourne et al. (2015) and references within.

Figure S11: Geochemical populations identified within shard analyses from the GIK23415-9 225-226 cm deposit. (i) inset of total alkali vs. silica plot. Division line to separate alkaline and sub-alkaline material from MacDonald and Katsura (1964). Chemical classification and nomenclature after Le Maitre et al. (1989). (ii) FeO/TiO$_2$ vs. SiO$_2$ and (iii) TiO$_2$ vs. Al$_2$O$_3$ compositional variation diagrams comparing populations to characterisations of proximal Icelandic material. Geochemical fields for Icelandic source volcanoes are based on those utilised in Bourne et al. (2015) and references within.
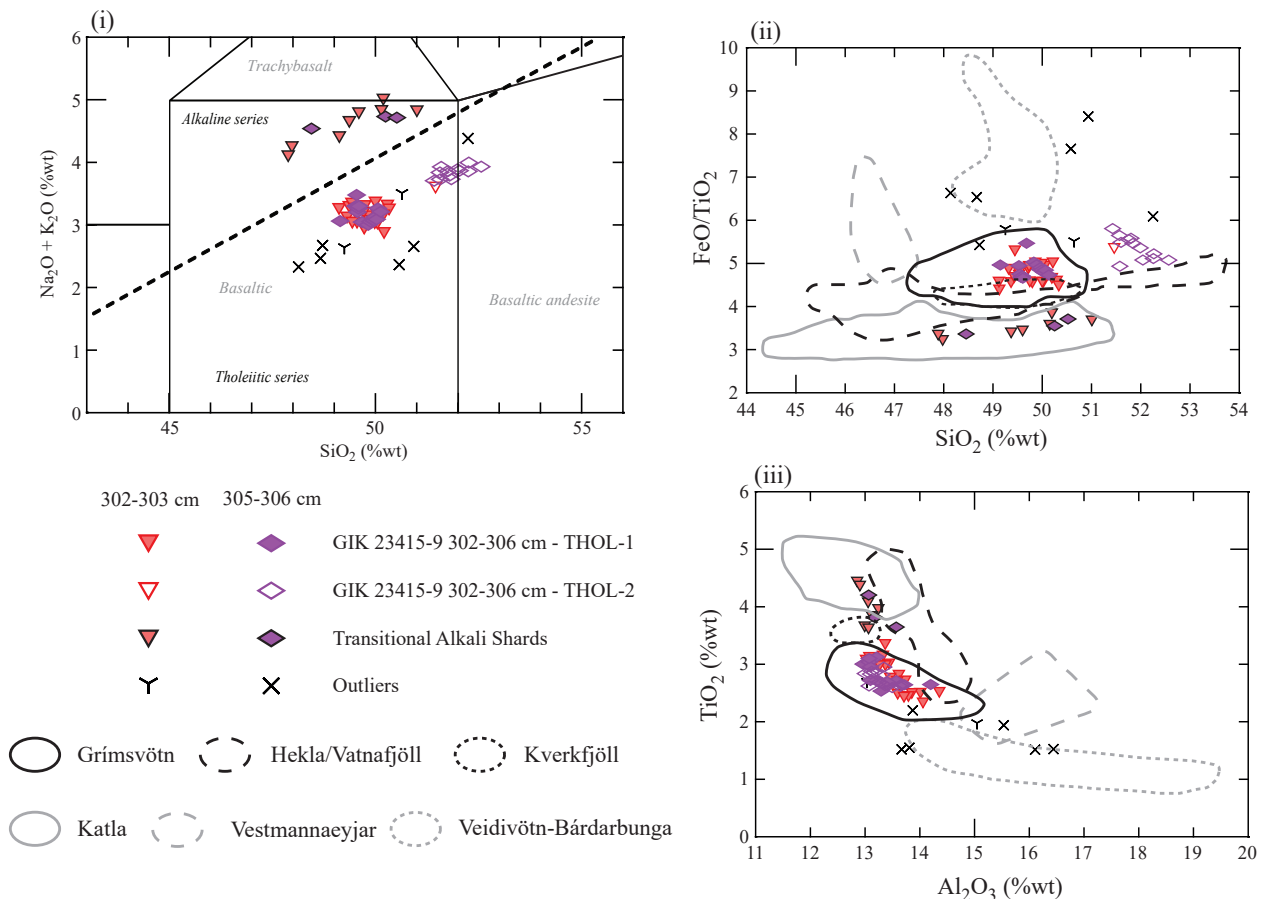

Figure S12: Geochemical populations identified within shard analyses from the GIK23415-9 302-306 cm deposit. (i) inset of total alkali vs. silica plot. Division line to separate alkaline and sub-alkaline material from MacDonald and Katsura (1964). Chemical classification and nomenclature after Le Maitre et al. (1989). (ii) FeO/TiO$_2$ vs. SiO$_2$ and (iii) TiO$_2$ vs. Al$_2$O$_3$ compositional variation diagrams comparing populations to characterisations of proximal Icelandic material. Geochemical fields for Icelandic source volcanoes are based on those utilised in Bourne et al. (2015) and references within.
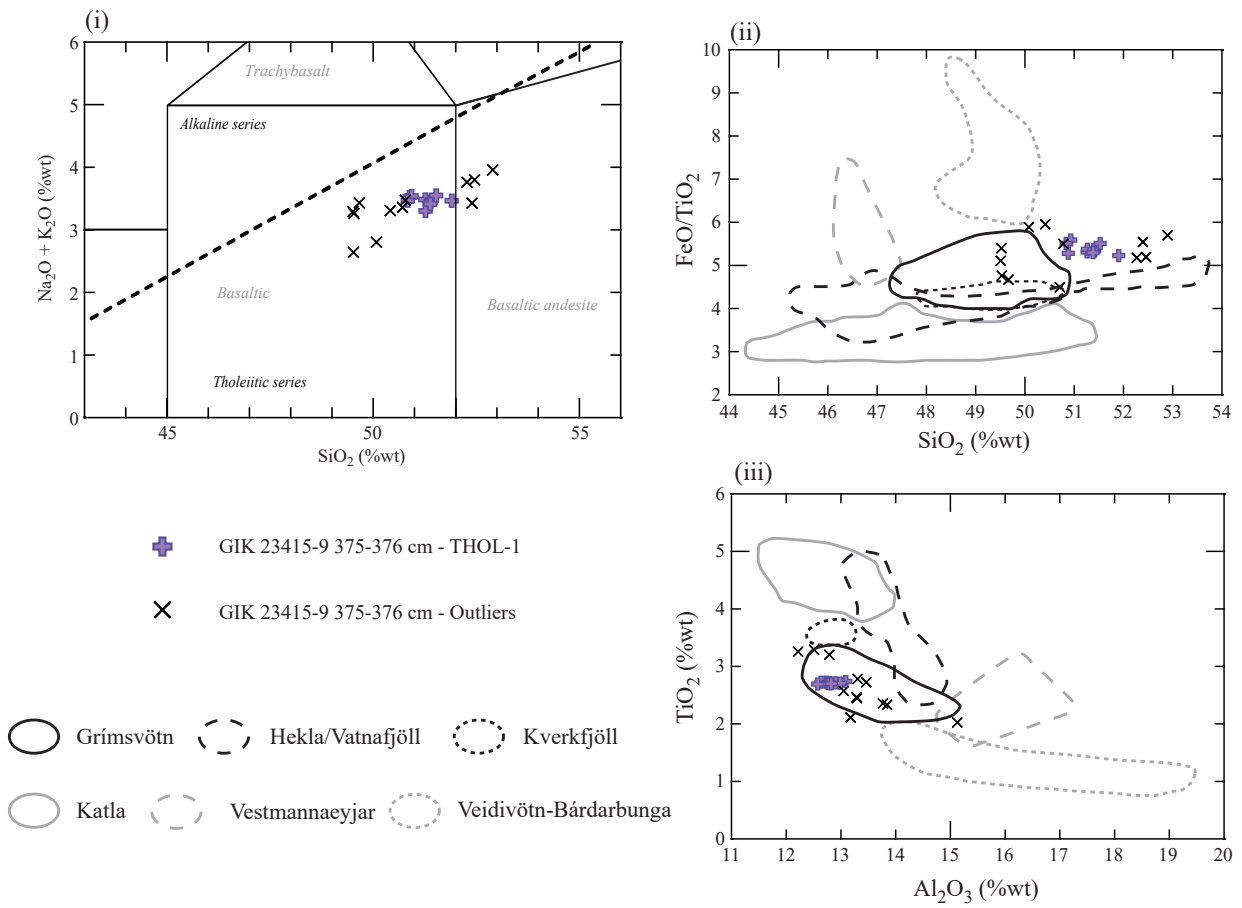
Figure S13: Geochemical populations identified within shard analyses from the GIK23415-9 375-376 cm deposit. (i) inset of total alkali vs. silica plot. Division line to separate alkaline and sub-alkaline material from MacDonald and Katsura (1964). Chemical classification and nomenclature after Le Maitre et al. (1989). (ii) FeO/TiO_2 vs. SiO_2 and (iii) TiO_2 vs. Al_2O_3 compositional variation diagrams comparing populations to characterisations of proximal Icelandic material. Geochemical fields for Icelandic source volcanoes are based on those utilised in Bourne et al. (2015) and references within.